STINFO COPY

AFRL-RW-EG-TR-2010-001

AUTONOMOUS AERODYNAMIC CONTROL OF MICRO AIR VEHICLES

Gregg Abate
Kelly Stewart
Judson Babcock

Air Force Research Laboratory
Munitions Directorate
101 W Eglin Blvd
Eglin AFB, FL 32542

October 2009

FINAL REPORT FOR PERIOD MARCH 2005 – SEPTEMBER 2009

AIR FORCE RESEARCH LABORATORY, MUNITIONS DIRECTORATE

■ **Air Force Materiel Command** ■ **United States Air Force** ■ **Eglin Air Force Base**

NOTICE AND SIGNATURE PAGE

Using Government drawings, specifications, or other data included in this document for any purpose other than Government procurement does not in any way obligate the U.S. Government. The fact that the Government formulated or supplied the drawings, specifications, or other data does not license the holder or any other person or corporation; or convey any rights or permission to manufacture, use, or sell any patented invention that may relate to them.

This report was cleared for public release by the 96 Air Base Wing, Public Affairs Office, and is available to the general public, including foreign nationals. Copies may be obtained from the Defense Technical Information Center (DTIC) <http://www.dtic.mil/dtic/index.html>.
.

AFRL-RW-EG-TR-2010-001 HAS BEEN REVIEWED AND IS APPROVED FOR PUBLICATION IN ACCORDANCE WITH ASSIGNED DISTRIBUTION STATEMENT.

FOR THE DIRECTOR:

//SIGNED//	//SIGNED//
MIKEL M. MILLER, PhD, DR-IV	GREGG L. ABATE, PhD, DR-III
Technical Director	Chief, Airframe Dynamics & Robust Control Section
Advanced Guidance Division	Weapon Dynamics & Controls Sciences Branch

This report is published in the interest of scientific and technical information exchange, and its publication does not constitute the Government's approval or disapproval of its ideas or findings.

REPORT DOCUMENTATION PAGE

Form Approved
OMB No. 0704-0188

1. REPORT DATE *(DD-MM-YYYY)*	**2. REPORT TYPE**	**3. DATES COVERED** *(From - To)*
19-10-2009	FINAL	MAR 2005 – SEP 2009

4. TITLE AND SUBTITLE
AUTONOMOUS AERODYNAMIC CONTROL OF MICRO AIR VEHICLES

5a. CONTRACT NUMBER
N/A

5b. GRANT NUMBER
N/A

5c. PROGRAM ELEMENT NUMBER
62602F

6. AUTHOR(S)
Gregg Abate
Kelly Stewart
Judson Babcock

5d. PROJECT NUMBER
2304

5e. TASK NUMBER
AM

5f. WORK UNIT NUMBER
10

7. PERFORMING ORGANIZATION NAME(S) AND ADDRESS(ES)

Air Force Research Laboratory
Munitions Directorate
101 W Eglin Blvd
Eglin AFB, FL 32542

8. PERFORMING ORGANIZATION REPORT NUMBER

9. SPONSORING / MONITORING AGENCY NAME(S) AND ADDRESS(ES)

SAME

10. SPONSOR/MONITOR'S ACRONYM(S)
AFRL-RW-EG

11. SPONSOR/MONITOR'S REPORT NUMBER(S)
AFRL-RW-EG-TR-2010-001

12. DISTRIBUTION / AVAILABILITY STATEMENT
DISTRIBUTION A: Approved for public release; distribution unlimited. 96th ABW/PA Approval and Clearance # 96ABW-2009-4092, dated 17 Nov 2009

13. SUPPLEMENTARY NOTES

14. ABSTRACT

This effort helped to solidify the linkage between the aerodynamic and guidance and control aspects of micro air vehicles. Micro air vehicles are characterized by small vehicle size (O 10 cm), low flight speeds (O 10 m/s), and low Reynolds number (O 10,000-100,000). These micro air vehicles (MAVs) are unique in the fact that they are inherently multi-functional systems. That is, sub-systems within the MAV perform more than one task. In this regard, aerodynamic and guidance and control aspects of the MAVs need to be developed in concert. New methods for guidance and control, such as vision-based and biometrically-inspired methods, will rely on detailed understanding of the MAV aerodynamic characteristics to be effective. This effort focused on the influence of flexible airframes to provide for a much more robust airframe for micro-class air vehicles. Results demonstrated that airframes with inherent flexibility are more tolerant to disturbances (i.e., gusts) and are better suited to relevant Air Force Missions. Future work will focus on the tuning of the vehicle structure and sensing of vehicle deformations to provide enhanced control.

15. SUBJECT TERMS

16. SECURITY CLASSIFICATION OF:			**17. LIMITATION OF ABSTRACT**	**18. NUMBER OF PAGES**	**19a. NAME OF RESPONSIBLE PERSON**
a. REPORT	**b. ABSTRACT**	**c. THIS PAGE**			Gregg Abate
UNCLASSIFIED	UNCLASSIFIED	UNCLASSIFIED	UL	70	**19b. TELEPHONE NUMBER** *(include area code)* 850 883 2596

Table of Contents

This page intentionally left blank

Abstract

This report presents research studies performed under the in-house research effort on Autonomous Aerodynamic Control of Micro Air Vehicles (MAVs). The report is organized in four appendices comprised of papers published during the course of the project.

This effort helped to solidify the linkage between the aerodynamic and guidance and control aspects of micro air vehicles. Micro air vehicles are characterized by small vehicle size (O 10 cm), low flight speeds (O 10 m/s), and low Reynolds number (O 10,000-100,000). These micro air vehicles (MAVs) are unique in the fact that they are inherently multi-functional systems. That is, sub-systems within the MAV perform more than one task. In this regard, aerodynamic and guidance and control aspects of the MAVs need to be developed in concert. New methods for guidance and control, such as vision-based and biometrically-inspired methods, will rely on detailed understanding of the MAV aerodynamic characteristics to be effective. This effort focused on the influence of flexible airframes to provide for a much more robust airframe for micro-class air vehicles. Results demonstrated that airframes with inherent flexibility are more tolerant to disturbances (i.e., gusts) and are better suited to relevant Air Force Missions. Future work will focus on the tuning of the vehicle structure and sensing of vehicle deformations to provide enhanced control.

The principal technical objective of this effort was to solidify aspects of various engineering disciplines that must be integrated for successful development of an autonomously controlled micro aerial vehicle. Operational motivation for this work was fueled by the need for increased situational awareness (especially in urban environments), remote sensing capability, “over the hill” reconnaissance, precision payload delivery, and aid in rescue missions.

Micro air vehicles can be considered a sub-class of uninhabited air vehicles (UAVs). UAVs have been developed in recent years by leveraging traditional aerospace science technologies. However, the engineering maturity required for MAV development has not kept pace. For instance, due to the extremely small size of MAVs, the flowfield is dominated by separated flow regimes on the order of the vehicle size. Also, the small size of MAVs gives rise to small inertias which make the MAV more susceptible to wind gusts.

Results of the research will benefit the Air Force in the design of future micro aerial vehicles. Mission scenarios are ever-evolving for this class of aerial vehicle and it is anticipated that future tactical MAVs will need to be tailored for specific needs and missions. In that regard, the ability to design and build such MAVs in a timely manner will be paramount. The results of this research effort will allow for rapid design and testing of such MAVs. The experience gained in characterizing MAV airframes, energy storage, material and sensor development, and G&C methodologies will allow for quick prototyping and design refinement. Testing of such designs in a realistic environment, such as urban canyons, will allow for rapid assessment of the MAVs as well. .

Results

The main focus of this effort centered on the effects of vehicle flexibility and its impact on flight mechanics and performance.

The term "Agility" is oft used to describe the capability required for future MAV systems. Simply put, we are talking about the ability of a MAV system to fly in cluttered environments, avoid obstacles, reject gusts, recover from disturbances and impacts, and land and take-off. In the extreme, this will require MAV systems to have the flight capabilities of natural fliers; namely birds, bats, and insects. One has most likely witnessed a bird performing a complex flight maneuver in order to avoid an obstacle or fly in a gusty environment. Likewise, who has not witnessed a fly impact a glass window only to recover and attempt to fly through the glass many more times? These and other examples represent performance ability for MAVs when we speak of Agility. The question, then, is how to we provide this capability for future MAV systems?

Flexibility, on the other hand, refers to the fact that the MAV structure (or parts of the structure) has a certain amount of designed flexibility that lends itself to deformations favorable to flight agility. An example of this is the small-scale shape changes that results from a bird's feathers bending that allow a bird to reject a gust or fly at high angles of attack (note that this is different from a bird being able to fold its wing which is considered morphing). This is best exemplified by pilots of radio-controlled MAVs that report MAVs with a "flexible" wing (i.e., covered in a latex material) are easier to fly than MAVs with a rigid wing[1]. It is reasonable to assume that for a MAV with a flexible wing, gust energy would be, to some extent, absorbed by the flexibility of the structure. This absorption of the energy (and subsequent dissipation) would reduce the amount of energy into moving the vehicle thereby reducing the impact of the gust. Additionally, Breuer, et al.[2] and Gursul et al.[3], have shown that airfoils which are compliant delay stall and reduce the separation region.

---

[1] Ifju, P., University of Florida, personal communication.

[2] Song, A. and Breuer, K., "Dynamics of a compliant membrane as related to mammalian flight," AIAA paper, 2007-0665. AIAA Aerospace Sciences Meeting, Reno NV 2007.

The impact of a flexible airframe on the response to disturbances was the subject of the first part of this efforts the results of which are presented in Appendix 1. Here, it is shown that the airframe exhibited different responses to disturbances and that the airframe damped quicker to disturbances. These results reinforce the observation that MAVs with a degree of flexibility are less susceptible to disturbances. So the questions that need to be addressed are (among others):

1. To what extend does vehicle flexibility violate the assumption of a rigid body airframe?
2. Can "flexibility" effects be added to the dynamic equations of flight and, if so, will it improve autonomous flight control?
3. Can sensors be added to the airframe to measure flexibility such that this information can be used by the flight control system?
4. Can the flexibility be modified during flight so as to change the flight performance?

The answer the question "To what extend does vehicle flexibility violate the assumption of a rigid body airframe?" was addressed by the work present in Appendix 1. The flight dynamic equations of motion (e.g., Etkin[4]) assume a rigid body in their development. Modifications to the mass properties of the airframe and the associated aerodynamic coefficients and stability derivatives as a result of vehicle flexibility were modeled and results show an effect on the flight performance. Clearly, an effect is present but to what extent this effect impacts the autonomous control is yet to be determined.

To further understand the effects of this flexibility and to assess the validity of the model incorporated in Appendix 1, a generic micro air vehicle model was designed which would serve as a test bed with which research can be applied and shared. This generic MAV is presented in detail in Appendix 2.

With a generic model established, flight hardware was produced to gather experimental data. This data is presented in Appendix 3. Here, the GENMAV model was used as a baseline configuration and hinges were added to the wing root and were attached with a spring-damper system. It is planned that future testing with this model will help validate the simulation developed for a "flexible" wing MAV so that future studies can focus on addressing the second

---

[3] Rojratsirikul P., Wang, Z., and Gursul, I., "Unsteady Aerodynamics of Membrane Airfoils," AIAA paper 2008-0613, AIAA Aerospace Sciences Meeting, Reno NV 2008.

[4] Etkin, B., "Dynamics of atmospheric flight," Dover Publications, 2005.

question presented above. Namely, can “flexibility” effects be added to the dynamic equations of flight and, if so, will it improve autonomous flight control?

Finally, the paper presented in Appendix 4 presents work in which the aerodynamic stability derivatives are evaluated for a pliant wing MAV. The MAV used in this study differs from the GENMAV configuration as this model proved too bulky to be tested within the facility. The resulst of this effort clearly indicate that flexibility needs to be considered when using pliant wings.

This page intentionally left blank

Recommendations

This effort has only just begun to study the linkage between aerodynamics and controls for enhanced MAV flight agility. Modeling is continuing on a flexible airframe concept to look at the effects of flexibility on flight control. In this effort a flying MAV model was developed, built, and flown that incorporates an articulated wing that matches the model under development. Flight tests have begun and data is being collected that will, hopefully, allow us to validate the model. Wind tunnel studies have also begun in which detailed aerodynamic quantification can be mad regarding MAV performance with flexible airframes. Understanding of the impact of flexible airframes will be crucial to development of enhanced flight control algorithms for MAVs. With a validated model, we can begin to look at control schemes for flexible vehicles as well as design and "tune" the flexibility for future MAV concepts.

This effort has clearly shown the importance of vehicle flexibility on flight performance of MAVs. If we review the 4 questions presented in the previous section, we can safely say that question number 1 has been adequately addressed and that question 2 has been partially addressed by the work of this effort. Clearly, the remaining questions need to be addressed if we hope to exploit the role of flexibility for flight control.

This page intentionally left blank

Appendix 1

Flight Mechanics and Control Issues for Micro Air Vehicles

This page intentionally left blank

Flight Mechanics and Control Issues for Micro Air Vehicles

Kelly Stewart*, Gregg Abate†, and Johnny Evers‡
Air Force Research Laboratory, Munitions Directorate, Eglin AFB, FL 32542-6810

Micro air vehicles (MAVs) pose unique challenges for autonomous controlled flight. MAVs are extremely small in size (~ 15 cm), slow in speed (~10 m/s), and light in weight (~ 100 gm). Additionally, their small size gives rise to low Reynolds number (~ 50,000) flight regimes where aerodynamic separation and unsteadiness are known to occur. The result is that MAVs are sensitive to small changes in flight conditions and atmospheric disturbances (i.e., wind gusts). Additionally, some classes of MAVs tend to have a high degree of structural flexibility due to packaging or aerodynamic considerations. For this class of MAV, aero-structural interaction is dominant which leads to changes in the vehicle's mass properties, aerodynamic coefficients, and stability derivatives. All these factors need to be considered in autonomous flight control development for MAVs. This paper presents initial results on the modeling of a generic MAV configuration with "flexible" wings which is a form of passive morphing. For this work, the MAV's wing dihedral is allowed to vary based upon vertical loading. The aerodynamics and mass properties for several fixed dihedral, symmetric wing airframe configurations are computed and integrated into a high fidelity 6DoF rigid body simulation. The open- and closed-loop responses of the MAV are compared to a MAV with fixed wings due to control doublets. The results indicate a slight reduction in the transient response to the control doublets for the flexible wing MAV versus the fixed wing MAV. However, a more detailed aero-structural model needs to be developed for detailed control development.

Nomenclature

ρ	=	air density
$\overline{\delta_a}$	=	cumulative aileron movement
$\Delta\delta_a$	=	incremental change in aileron deflection
$\overline{\delta_e}$	=	cumulative elevator movement
$\Delta\delta_e$	=	incremental change in elevator deflection
Γ	=	dihedral angle
ϕ, θ, ψ	=	Euler angles [roll, pitch, yaw]
η_P	=	propeller efficiency
ω_P	=	rotational speed of propeller
b	=	wing span
c	=	chord
C_D	=	drag coefficient
C_L	=	lift coefficient
$C_{l\beta}$	=	roll moment versus sideslip stability derivative
C_m	=	pitch moment coefficient
$C_{m\alpha}$	=	pitch moment versus angle-of-attack stability derivative
$C_{n\beta}$	=	yaw moment versus sideslip stability derivative
C_P	=	power coefficient

* Aerospace Engineer, AFRL/MN, Member, AIAA
† Team Lead, Autonomous Control Team, AFRL/MN, Associate Fellow, AIAA
‡ Senior Researcher, AFRL/MN, Senior Member, AIAA

d_P	=	propeller diameter
F_z	=	normal force
g	=	gravitational acceleration
$\overline{H}$	=	angular momentum vector
I_P	=	propeller moment of inertia about the x-axis
I_{xx}, I_{yy}, I_{zz}	=	principal moments of inertia
I_{xz}	=	product of inertia pertaining to the x-z plane
k_P	=	number of propeller blades
m	=	vehicle mass
m_P	=	propeller mass
n_z	=	vertical load factor
P	=	power
p, q, r	=	body rates [roll, pitch, yaw]
T	=	thrust
V	=	airspeed
$Z_{C.G.}$	=	location of center of gravity along the z-axis

I. Introduction

In recent years, the Air Force Research Laboratory Munition Directorate (AFRL/MN)[1] has had an active research program in many areas of micro aerial vehicle (MAV) development. MAVs are characterized by small vehicle size ($\mathcal{O}$ 10 cm), low flight speed ($\mathcal{O}$ 10 m/s), and low Reynolds number ($\mathcal{O}$ 10,000-100,000). The desire to develop MAVs is fueled by the need for increased situational awareness (especially in urban environments), remote sensing capability, "over the hill" reconnaissance, precision payload delivery, and aid in rescue missions. Figure 1 depicts where MAVs lay on the mass versus Reynolds number plot for flight vehicles and Figure 2 depicts some examples of MAVs. MAVs can be considered a sub-class of uninhabited air vehicles (UAVs). UAVs have been developed in recent years by leveraging traditional aerospace science technologies. However, the scientific and engineering disciplines that are well understood and employed in larger UAV development do not scale linearly or proportionally with decreased size. For instance, a MAV that is 50% the size of a larger UAV will have a mass that is ~88% smaller and moments of inertia that are ~97% smaller than that of the full size UAV. The air loading for MAVs becomes much smaller as a result and this leads to very lightweight MAV designs. These light air vehicles are now very susceptible to gusts.

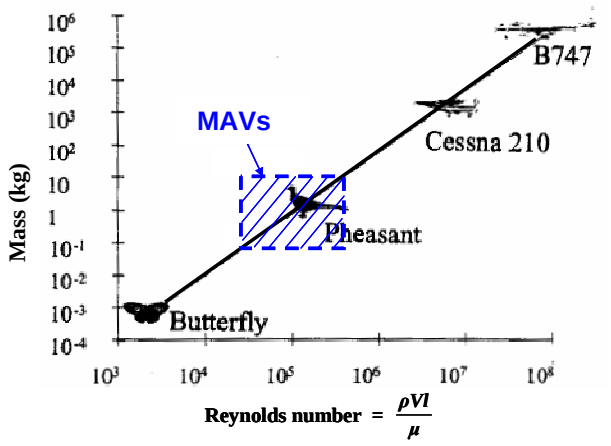

Figure 1. Mass versus Reynolds number for MAVs[2]

Figure 2. Examples of MAVs

Two aspects of MAV development that are of particular interest to the Munitions Directorate are that of "aerodynamic agility" and "robust controllability". Aerodynamic agility provides a MAV the ability to maneuver in close quarters. Robust controllability allows a MAV to be controlled in a variety of methods and circumstances. Simply put, AFRL is interested in autonomous aerodynamic control of MAVs. This requires the ability to properly

characterize the aerodynamics of such MAVs for use in the design of vehicle control systems that will allow the vehicles to operate under limited human supervision in uncertain or hostile environments.

Of particular concern are the issues of flight mechanics and flight control for MAVs. An important assumption is that of a rigid vehicle in the well established development of air vehicle flight mechanics[3]. As was previously mentioned, MAVs are extremely light weight and sensitive to wind and gusts. One way to help alleviate this problem is to allow the MAV to have a high degree of vehicle flexibility. In this manner, the energy of the wind and gusts can be absorbed by the airframe to help minimize the gross movement of the vehicle. This passive response to a disturbance may allow improved flight performance of a MAV. There are also aerodynamic advantages associated with flexible wings which may help improve MAV flight characteristics[4, 5].

The aim of this paper is to look at the issue of air vehicle flexibility on the flight mechanics and control aspects particular to MAVs. It is assumed that the flexibility of the airframe is sufficient to change the aerodynamic and inertia characteristics of the MAV and that this deformation is solely a result of air loading. Of particular interest for this study is to investigate the effect of flexible body dynamics on the MAV flight performance. Future studies will explore control design issues associated with exploiting the effects of vehicle flexibility to yield increased vehicle agility.

II. Simulation

A. Simulation Architecture

The studies in this paper were carried out using a simulation based upon the Computer Aided Design of Aerospace Concepts (CADAC)[6] architecture. This simulation architecture is written in C++ and employs a modular scheme where different models representing different aspects of an air vehicle work together. The simulation can be tailored to represent a specific airframe by swapping out data sets that define the aerodynamic coefficients and mass properties. Within the data sets, aerodynamic coefficients are separated into look-up tables of stability, dynamic, and control derivatives.

Models that make up the simulation include the equations of motion for a rigid body vehicle, an aero-adaptive autopilot, a reciprocating motor, and a linear guidance law. In the simulation, the kinematic and dynamic equations feed into each other as depicted in Figure 3. Items in blue indicate additions made by the author of this paper.

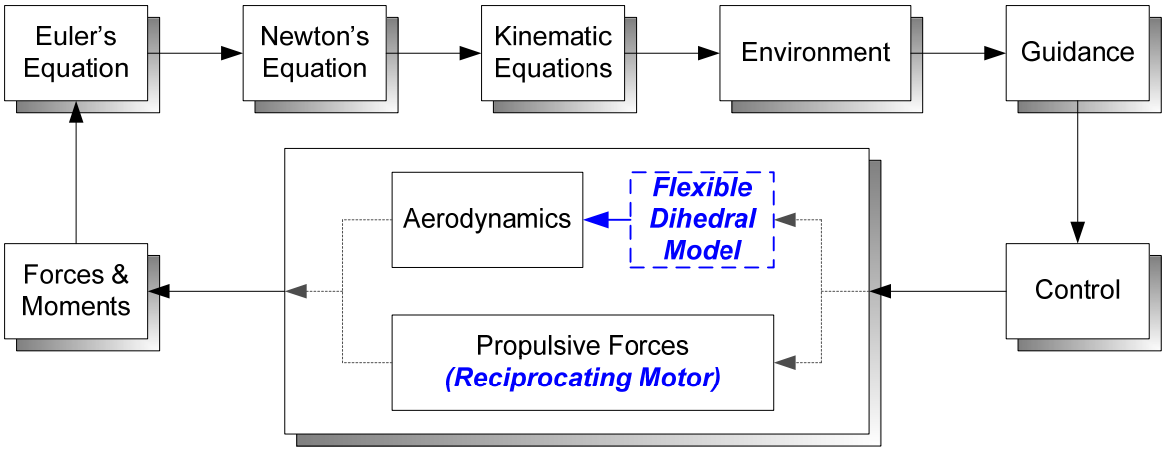

Figure 3. Layout of the models comprising a 6-DOF simulation[6,7].

The fact that the simulation architecture is laid out in a modular form gives the user the flexibility needed to modify the simulation to current needs, including adding additional models if need be. Existing models can easily be modified without having to rewrite the entire simulation, which allows the user to represent a vehicle with as much or as little detail as they wish. It is for this ease of customization that such an architecture was chosen as the basis for a six-degree-of-freedom MAV simulation.

B. Micro Air Vehicle Model

For this paper, a generic airframe was designed that would provide a baseline for this research. The design is similar to existing MAVs. The airframe has a conventional aircraft design to allow for easy determination of aerodynamic coefficients and stability derivatives and minimal changes to the simulation code. The resulting design has a 2-ft wingspan, conventional controls, and flies around 30 mph. A diagram of the vehicle airframe is provided in Figure 4.

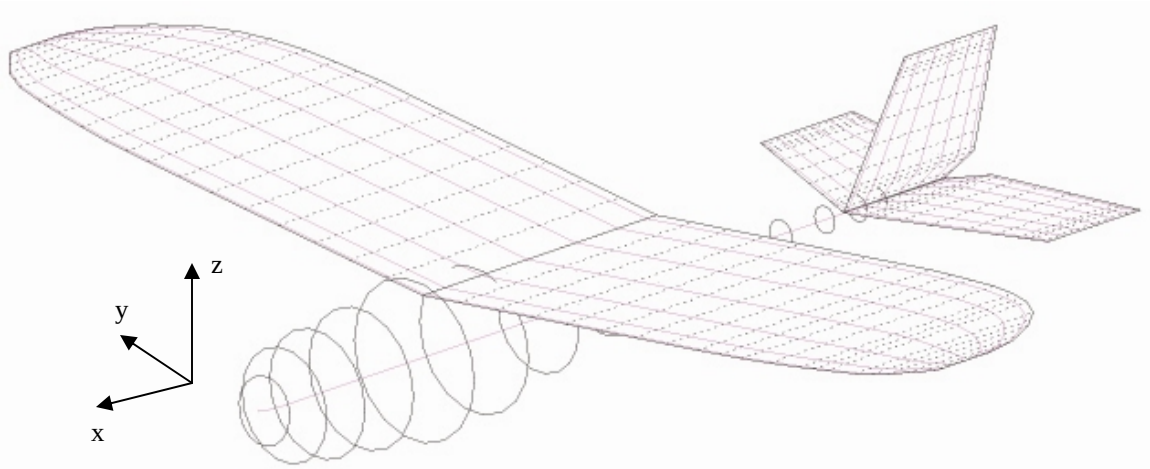

Figure 4. Diagram of the micro air vehicle model used for this paper. Note the circular fuselage, conventional tail fins, and thin wings. Not shown in this diagram is the camber of the wings and their incidence angle to the body.

1. Aerodynamics

Aerodynamic coefficients for the airframe were estimated using Athena Vortex Lattice (AVL), version 3.15[8]. As the name implies, this code uses the vortex panel method which works best for predicting the coefficients of thin lifting surfaces at small angles-of-attack and sideslip. Developers of AVL note that this code assumes quasi-steady flow defined by the following limits on the non-dimensional body rates:

$$\left|pb/2V\right| < 0.10, \quad \left|qc/2V\right| < 0.03, \quad \left|rb/2V\right| < 0.25 \tag{1}$$

These limits are typically not exceeded in normal flight by conventional aircraft; however, it is not uncommon for a MAV to surpass the limits due to its low inertia. While collecting data from the simulation for various maneuvers, checks were made to identify when the air vehicle exceeded such limits and an attempt was made to soften the maneuver. Wind tunnel data for a similar sized MAV[9] were compared to ensure the estimates given by AVL were reasonable and are shown in Figure 5. Here, the lift and drag coefficients are in general agreement but the pitching moment coefficient did not compare as well. However, an exact match was not deemed necessary for the purpose of this paper, rather, the comparison gave confidence in AVL's estimates and the user's understanding of how to work with AVL.

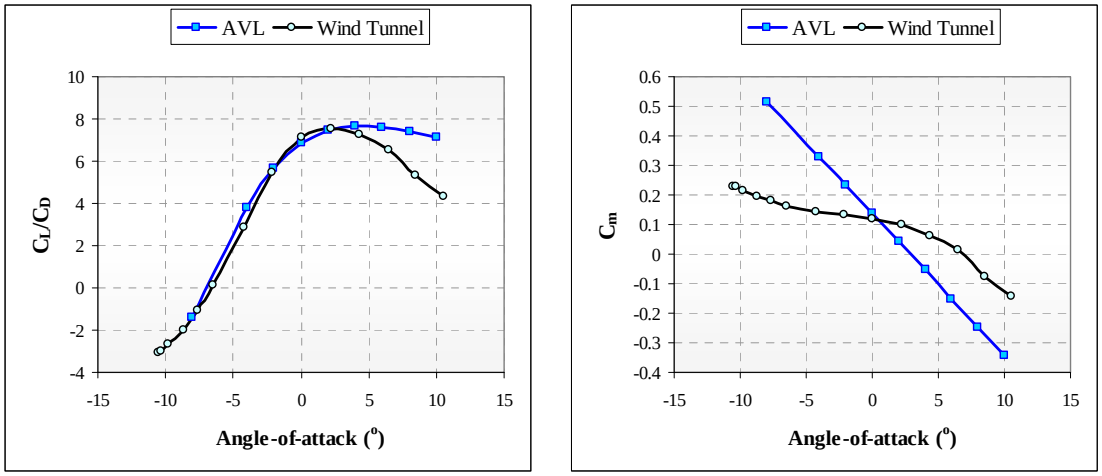

Figure 5. Comparison of AVL-predicted aerodynamic coefficients versus angle-of-attack with wind tunnel data[9] for the MAV model.

The modeling of the flexible wing was accomplished by a set of fixed dihedral configurations. Aerodynamic data was then determined for each fixed dihedral. Wing deflection is assumed to be symmetric and is discussed in further detail in section III-A. The nominal dihedral value is 7°, based on the dihedral angle of the vehicle detailed in Reference 9. Selection of the other five dihedral angles was purely arbitrary and is listed as follows: -5°, 0°, 10°, 20°, and 30°. These six values will be referred to as the dihedral breakpoints throughout the rest of this paper. Figure 6 through Figure 9 show some of the aerodynamic data for each configuration as a function of dihedral angle.

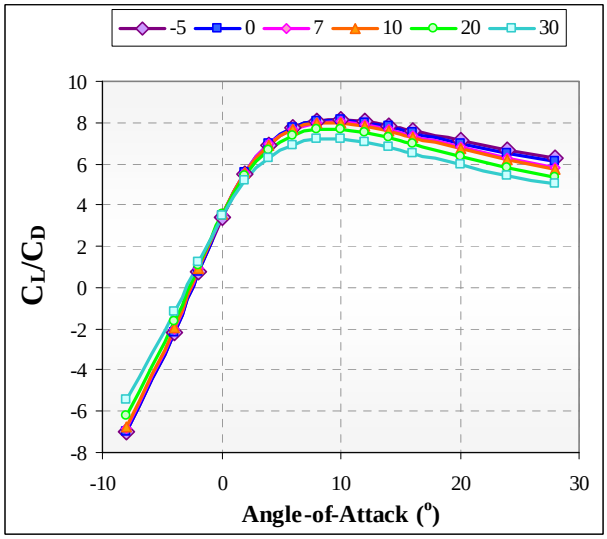

Figure 6. Lift-to-drag curve versus angle-of-attack for each of the dihedral angles as predicted by AVL for the MAV model.

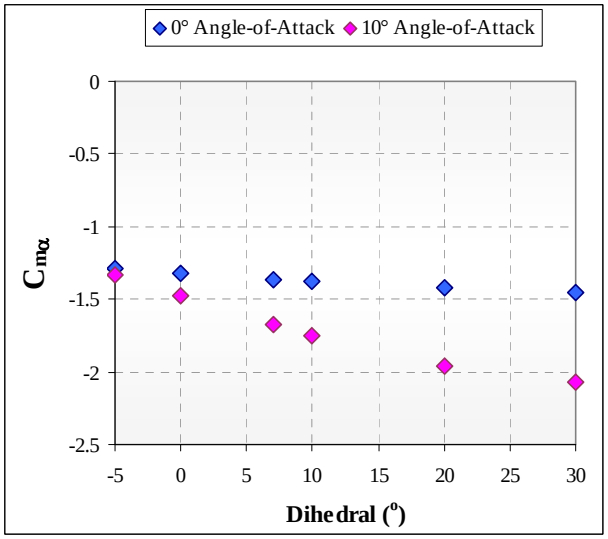

Figure 7. Pitch moment derivative versus dihedral angle as predicted by AVL for the MAV model.

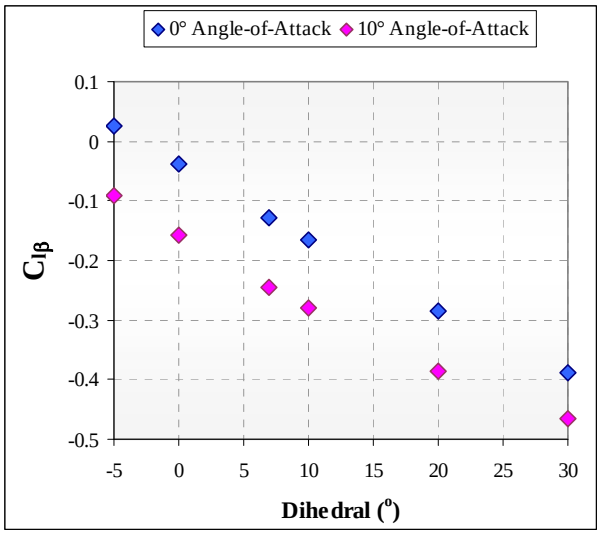

Figure 8. Roll moment derivative versus dihedral angle as predicted by AVL for the MAV model.

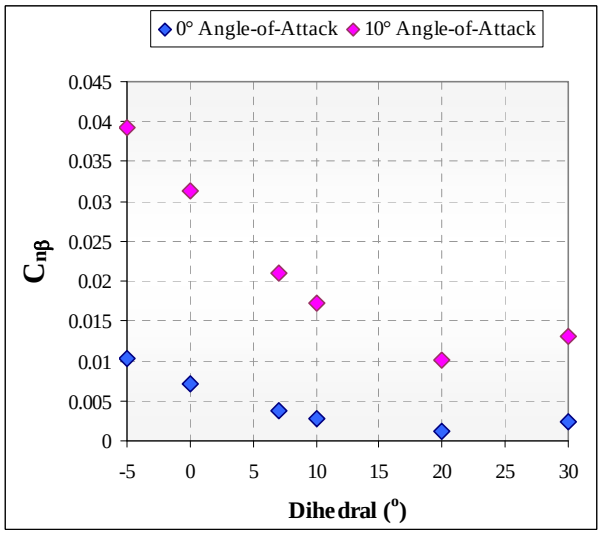

Figure 9. Yaw moment derivative versus dihedral angle as predicted by AVL for the MAV model.

2. Mass Properties

Each MAV configuration has its own inertia matrix due to the dihedral angle change. The inertia matrices were estimated using a spreadsheet along with the mass properties functionality of AVL. Major components of the air vehicle were approximated as basic geometric shapes for which the individual center of gravity and moments-of-inertia (MOI) were calculated, except for the fuselage. The fuselage MOI comes from the LODST[10] software package. Each of the MOI are calculated about the center of gravity of the component to which they pertain. A summary of the MOI calculation is provided in Table 1.

Table 1. Methods by which moments-of-inertia were computed for various components of the MAV model.

Vehicle Component	**Fuselage**	**Wings**	**Horizontal Tail**	**Vertical Tail**	**Propeller**	**Internal Equipment**
Approximation of MOI	**LODST Software**	**Flat Plate**	**Flat Plate**	**Flat Plate**	**Flat Disc**	**Cylinder**

These centers of gravity and MOI are input into AVL to calculate the entire inertia matrix via summation and the parallel axis theorem. To generate a new inertia matrix for a new dihedral, the vehicle's center of gravity is updated based on the new center of gravity of the wings along the z-axis. Due to the symmetric wing deflection, there is no center of gravity change in the x or y-axes. The change in the vehicle center of gravity is propagated through all the center of gravity locations, which are then updated in AVL. Table 2 provides the mass properties for each MAV configuration.

Table 2. Mass and Inertia properties of the MAV model for each dihedral angle.

Dihedral	$Z_{C.G.}$ (m)	I_{xx} (kg-m^2)	I_{yy} (kg-m^2)	I_{zz} (kg-m^2)	I_{xz} (kg-m^2)
-5°	**8.51×10^{-3}**	**1.93×10^{-3}**	**3.24×10^{-3}**	**4.81×10^{-3}**	**-7.48×10^{-5}**
0°	**9.93×10^{-3}**	**1.95×10^{-3}**	**3.26×10^{-3}**	**4.82×10^{-3}**	**-8.76×10^{-5}**
7°	**1.19×10^{-2}**	**1.98×10^{-3}**	**3.30×10^{-3}**	**4.80×10^{-3}**	**-1.02×10^{-4}**
10°	**1.28×10^{-2}**	**1.99×10^{-3}**	**3.32×10^{-3}**	**4.80×10^{-3}**	**-1.10×10^{-4}**
20°	**1.55×10^{-2}**	**2.03×10^{-3}**	**3.42×10^{-3}**	**4.73×10^{-3}**	**-1.32×10^{-4}**
30°	**1.81×10^{-2}**	**2.25×10^{-3}**	**3.56×10^{-3}**	**4.62×10^{-3}**	**-1.52×10^{-4}**

3. Propulsion Model and Engine Angular Momentum

A propeller engine is used by the MAV and is modeled within the simulation. The same wind tunnel test data[9] used to verify the AVL aerodynamic coefficients also includes propulsion data, specifically the coefficients of thrust and power. These coefficients were computed for a variety of angles-of-attack, airspeeds, and propeller rotation speeds. From this data, a look-up table of power coefficients was created. Thrust is calculated using the standard propulsion equations for reciprocal engines based on power and propeller efficiency[11]. An efficiency of 0.6 was chosen based on an average of the calculated values at 30 mph and angle-of-attack of 8°. This provided a reasonable and conservative estimate.

$$P = C_P \rho \left(\varpi_P / 2\pi \right)^3 {d_P}^5 \tag{2}$$

$$T = P \eta_P / V \tag{3}$$

This propulsion model also calculates the propeller angular momentum to capture the effects of the propeller in the air vehicle's roll moment. The propeller angular momentum is approximated as a sum of the MOI of the individual propeller blades about the propeller's axis of rotation, multiplied by the rotation speed.

$$I_P = m_P \sum^{k_P} {d_P}^2 / 4 \tag{4}$$

This value is then added to the angular momentum of the air vehicle about the roll axis. Several assumptions are required for representing the propeller contribution in this form: 1) the propeller rotational speed is much greater than the vehicle's roll rate, 2) the MOI of the propeller is much less than the MOI of the airplane and, 3) the mass of the propeller times its distance squared from the vehicle's center of mass is very small. For this MAV, these assumptions are valid and the given equation for the total angular momentum of the air vehicle holds.

$$\overline{H} = \begin{bmatrix} I_{xx} p + I_{xz} r + I_P \varpi_P \\ I_{yy} q \\ I_{zz} r + I_{xz} p \end{bmatrix} \text{(Ref. 7)} \tag{5}$$

III. Passive Dihedral Response

The variation in dihedral angle is considered a passive response of the vehicle due simply to vertical loading of the vehicle. The change of dihedral is also forced to be symmetric for this study. Both open-loop and closed-loop response of the MAV are considered.

A. Flexible Dihedral Model

By modeling the dihedral response as a function of vertical loading, the direction in which the dihedral changes treats the vertical loading as an aerodynamic force acting on the wings, rather than an inertial force acting on the vehicle's center of gravity. See Figure 10 below.

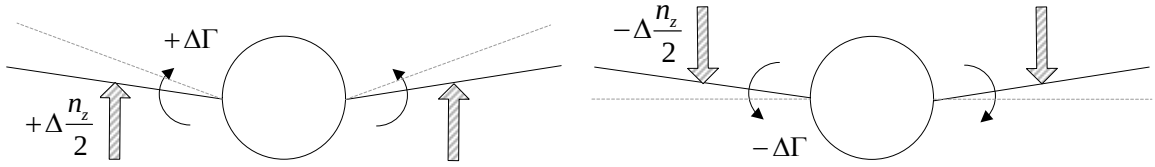

Figure 10. Direction of dihedral change induced by vertical loads

This assumes the vehicle can be approximated as a rigid body with the wings contributing the most to the normal force experienced by the entire vehicle. As such, the load acting on each wing is approximated as one half of the vehicle's vertical loading. Currently, the change in dihedral is symmetric; individual wing loads have not yet been taken into account. The change in the vertical load factor experienced by the vehicle when it departs from straight and level flight is given below,

$$n_z = {F_z}/{mg} - \cos\theta\cos\phi \text{ (Ref. 12)} \tag{6}$$

For the above equation, n_z will equal zero during straight and level flight, which corresponds to a vertical load factor of 1-g. Non-zero values of n_z will result in a change from the nominal dihedral angle according to the following relation,

$$\Gamma = (6°)n_z + 7° \tag{7}$$

This relation treats the joint of the wing and the aircraft as a hinge with no damping, the dihedral change is purely proportional to the vertical load. The selection of a slope equal to 6° is arbitrary and not supported by any structural modeling. Rather, it was determined via trial by allowing the dihedral to change enough for the analysis to be performed without the air vehicle going unstable during flight. Within the simulation, the change in dihedral is stepwise and matches with one of the six dihedral breakpoints. If equation 7 yields a dihedral angle not equal to one of the dihedral breakpoints, the simulation will use the aerodynamic data set of the nearest dihedral breakpoint of lower value. Thus, this simplified model treats the aerodynamics and mass properties associated with dihedral changes as piecewise step changes with no overshoot and no transients associated with the step changes. Figure 11 shows the dihedral steps according to the change in the vertical load factor, as implemented in the simulation.

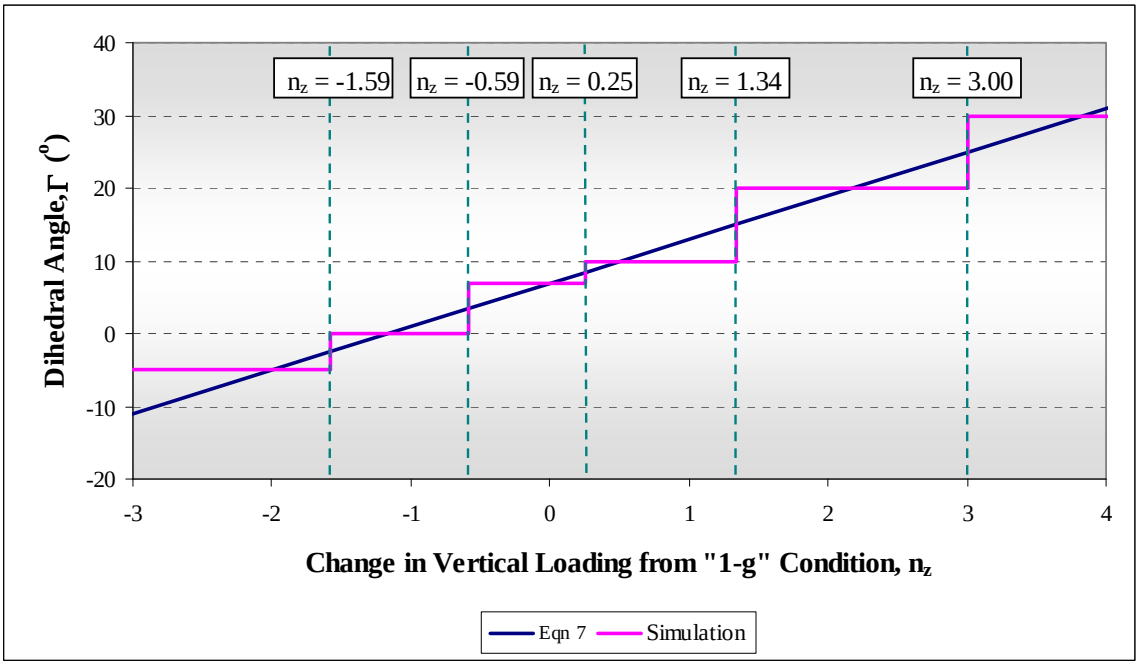

Figure 11. Step change of the dihedral angle for the corresponding change in vertical load factor.

B. Flexible versus Fixed Dihedral

A variety of maneuvers were considered when looking at the effect of passive dihedral response on the flight mechanics and control of the vehicle. Simple maneuvers such as a controlled dive with roll and small waypoint missions were investigated. The idea was to compare the dynamic response of the vehicle, response to autopilot commands, and activity of the control surfaces between the fixed and flexible dihedral configurations. Initial review of the data was inconclusive however. Even though control surfaces were slightly more active for the flexible dihedral cases, it was difficult to understand whether this was due to the changing dihedral or the nature of the autopilot. Being an aero-adaptive autopilot inherent in CADAC, the control loops use the pole-placement technique based on the aerodynamic derivatives and gains set by the user. The user-set gains remain the same, but gains calculated from the aerodynamic derivatives update with the changing dihedral. As such, it was decided to focus on both the open-loop dynamics of the vehicle due to doublet inputs as well as the closed-loop response to fast maneuvers.

1. Open-loop Response

Doublets in roll, pitch, and yaw were examined when studying the open-loop dynamics. For all three doublets, the aircraft was initialized at typical cruise speed, 13.4 m/s, and altitude, 61 m. To aid in trimming the aircraft, the autopilot was allowed to run for the first 15 seconds of flight. At 20 seconds into the flight, with the autopilot having been turned off, the doublet is performed. The control surface deflections associated with each of the doublets is listed as follows: ± 15° aileron for the roll doublet, ± 14° elevator for the pitch doublet, and ± 6° rudder for the yaw doublet. Deflections were held for 0.5 sec in each direction and then returned to trim position. The order of deflections was positive followed by negative. The magnitude of the deflections is based on the largest deflection possible without causing exceptionally large angle-of-attack or sideslip values to occur. Dihedral angle and vertical loading data gathered during each of the doublets are presented in Figure 12 and Figure 13. Recall that the vertical loading dictates how much the dihedral of the MAV will change from the nominal position of 7^o. Notice also that lateral maneuvers, such as the roll and yaw doublets, do yield a change in the vertical load factor due to cross-coupling of the flight equations of motion but, unlike the pitch doublet, the magnitudes are much smaller.

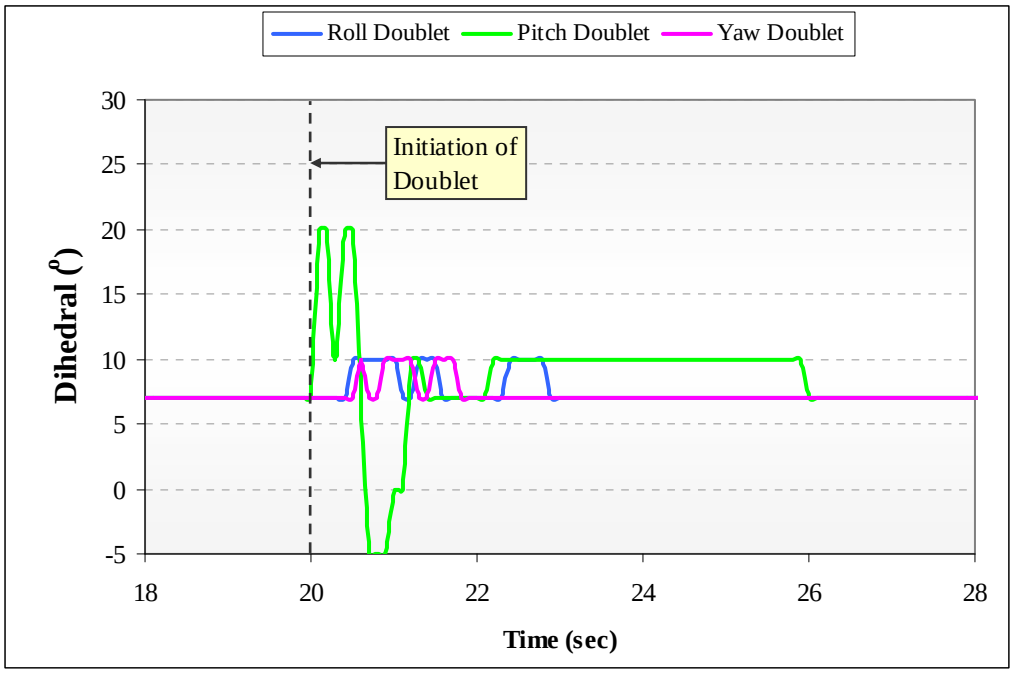

Figure 12. Dihedral angle versus time for control doublets.

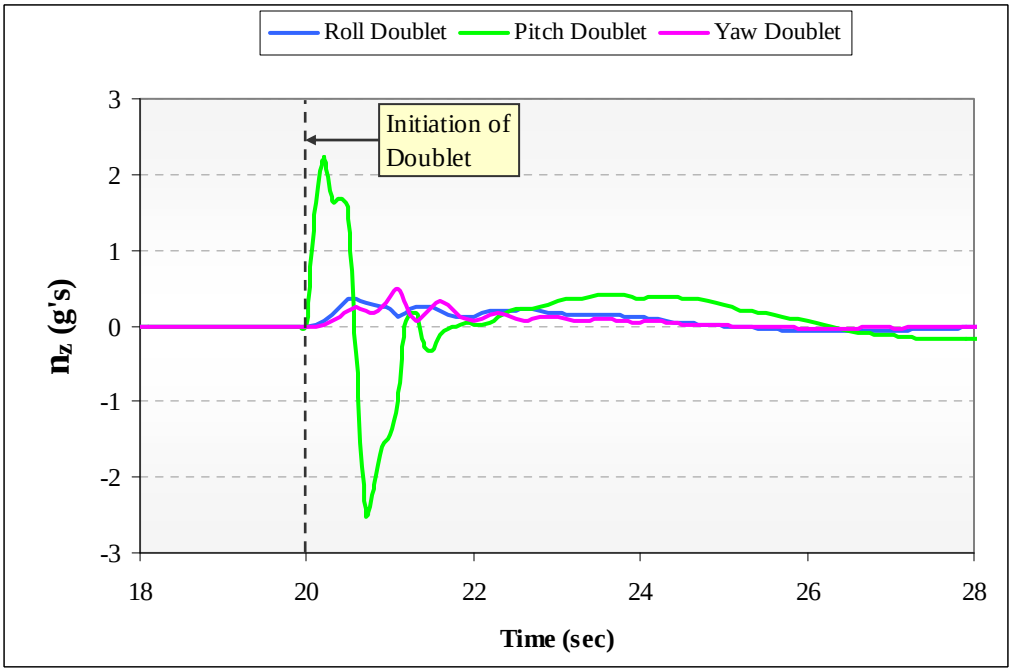

Figure 13. Vertical loading versus time for control doublets.

As can be seen from the above figures, the pitch doublet yielded the largest change between fixed versus flexible configuration with a magnitude slightly over ±2g's. This is due to the fact that the vertical loading is in the pitch plane. The change in vertical loading due to roll and yaw doublets occurs because of the cross-coupling between the stability axes and the influence of the propeller disk (see Equation 5). Referring back to the earlier discussion of vertical loading, it was mentioned that individual wing loading is not captured. Rather, the vertical loading on the entire vehicle is used to approximate the vertical loading upon the wings, i.e. both wings experience equal amounts

of loading and would therefore deflect the same amount simultaneously. The normal force acting on the entire vehicle feeds into the calculation of the vertical loading. If there is not a large change in the normal force, then there is not much change in the dihedral angle and, thus, not much change in response (refer back to Figure 10).

Since the pitch doublet causes the largest change in vertical loading and, hence, dihedral angle, the remainder of this discussion will focus on that maneuver. Figure 14 shows the dihedral angle from the initiation of the doublet to 8 seconds afterwards. The dihedral motion settles out after 6 seconds at which time the change in vertical loading on the aircraft from the nominal 1-g is minimal (see Figure 13). During the transient response, the greatest effect is observed in the lateral channels. This can be seen in Figure 16 and Figure 17. Notice how the response of both the fixed and flexible configurations line up closely in angle-of-attack, but differ in roll angle and sideslip.

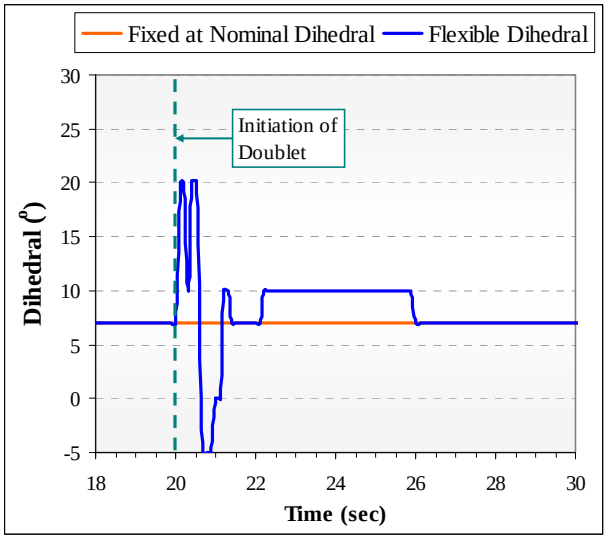

Figure 14. Dihedral angle variation versus time during a pitch doublet for a fixed and flexible MAV configuration.

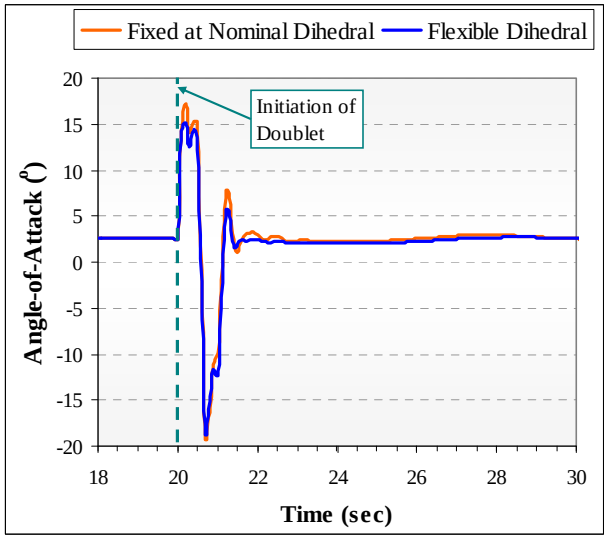

Figure 15. Angle-of-attack variation versus time resulting from a pitch doublet for a fixed and flexible MAV configuration.

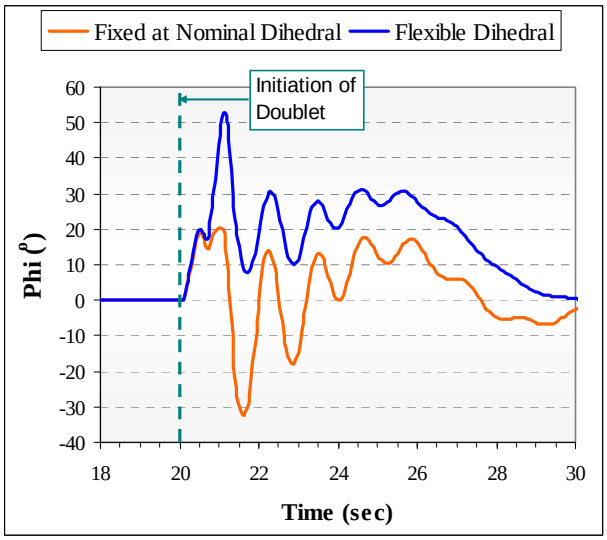

Figure 16. Roll angle response versus time resulting from a pitch doublet for a fixed and flexible MAV configuration.

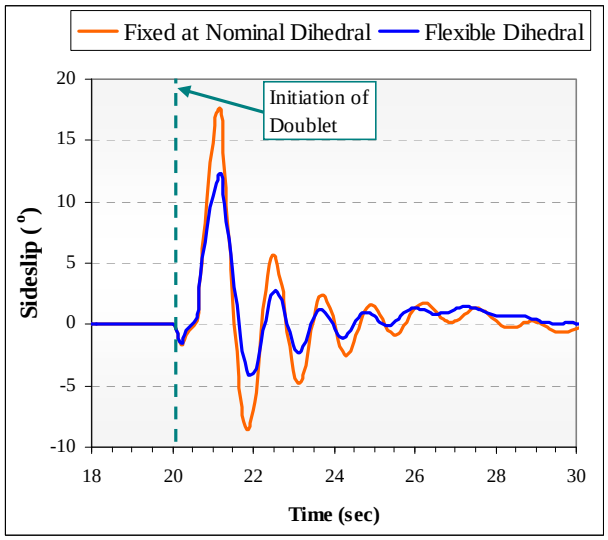

Figure 17. Sideslip variation versus time resulting from a pitch doublet for a fixed and flexible MAV configuration.

As mentioned, the vehicle response in the roll and yaw planes due to a pitch doublet is due largely to the propeller disk. However, it is seen that the response of the flexible wing MAV is lower in magnitude and damps out quicker. This is due to the changing of the dihedral which has a great influence on the cross-coupled stability derivatives ($C_{l\beta}$ and $C_{n\beta}$). Note how sideslip angle (β) damps quicker for the flexible-wing configuration. Again, this can be traced back to the behavior of the coefficients as a function of dihedral. In the 6-second time period following the doublet, sideslip for the fixed-wing configuration ranged from 17.5° to -8.6°. For the flexible-wing configuration, sideslip ranged from 12.3° to -4.0°. The flexible-wing MAV happened to be at a 10° dihedral angle for 80% of that time, which resulted in greater roll static stability (again, see Figure 8). This poses the question of whether such effects could potentially be useful in MAV control. Based on this, the results indicate that the flexibility of the vehicle tends to increase the damping of the transient response. The lack of variation in angle-of-attack between the fixed and flexible MAV configuration is due to the relative insensitivity of the pitch moment stability derivative ($C_{m\alpha}$) with dihedral angle (see Figure 7).

Note also the change in roll angle due to the flexible-wing MAV versus the fixed-wing MAV as shown in Figure 16. During the time period of 20.5 to 21 seconds, the roll angle for the flexible-wing configuration increased to 52° whereas the fixed-wing stopped at 20°. In the time period immediately after the pitch doublet, the flexible-wing MAV was experiencing a -5° dihedral which corresponds to an unstable[13] $C_{l\beta}$ (see Figure 8). Even though this instability exists only for a brief amount of time, it was enough to significantly increase the roll response.

2. Closed-loop Response

As mentioned earlier, a number of closed-loop maneuvers were performed for both the fixed and flexible dihedral. Having observed that a significant change in vertical loading on the aircraft is required for a dihedral change (due to how it is currently modeled), two missions were studied: 1) a dive at a constant bank angle and 2) a simple waypoint mission with changing altitude. In both cases, there were short periods, on the order of a few seconds, of noticeable difference in aileron and elevator activity. However, the two control surfaces nearly mirrored each other for most of the mission length. This can be attributed to several factors. The first would be the nearly constant dihedral angle for most of the flight time. Even though the aerodynamic coefficients vary with the dihedral angle, the dihedral angle only changed due to dynamic response. As a result, the MAV spends most of its time at the nominal dihedral, portraying the fixed and flexible-wing as essentially the same aircraft. Secondly, the simulation is "perfect" in that no noise or wind gusts are currently modeled. Wind gusts would allow for the dihedral to deflect more frequently during a maneuver and perhaps significantly alter the response between the two MAV configurations. Third, the symmetric deflection of the wings, as discussed in the preceding section, limits a change in dihedral to maneuvers involving significant changes in the vertical load acting on the air vehicle as a whole.

Despite the similarities recorded for most of the mission lengths, it is worth looking at those short time periods of noticeable differences. In both missions, the same trend regarding the difference in aileron and elevator activity was seen. The dive at a constant bank angle had the more noticeable differences of the two missions, so the following discussion will focus on details of that particular one. A plot of the passive dihedral response and a description of the maneuver setup are given in Figure 18.

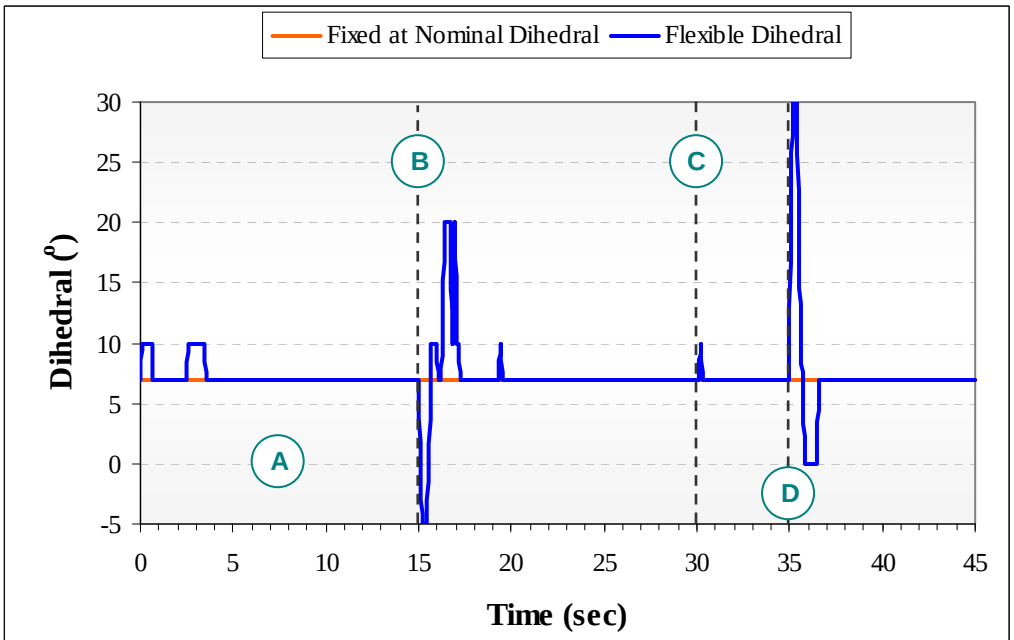

A - Air vehicle is trimmed at 61-m altitude and 13.3-m/s airspeed.
B - Simultaneous dive and roll is initiated. Air vehicle is commanded to hold a 21° bank angle.
C - Air vehicle is commanded to resume a 0° bank angle.
D - Air vehicle halts descent and begins to ascend.

Figure 18. Passive dihedral response that occurs during transitional periods for a dive maneuver.

Most of the dihedral activity occurs during the initiation of the simultaneous dive and roll and during the transition from descent to ascent. This makes sense in regards to how the dihedral deflection is modeled - the normal force must change significantly in order for the dihedral to change. Notice that the dihedral deflections only make up about 5.6 seconds (or 12.4%) of the entire mission length. This demonstrates how the fixed and flexible-wing configurations behave essentially like the same vehicle for most of the mission. To compare aileron and elevator activity between the two configurations, the amount of deflection for the two control surfaces was summed for mission points B, D, and the entire mission length. See equation 8, where n is the total number of time steps. The results are portrayed in Table 3.

$$\overline{\delta_a} = \sum_{i=1}^{n} \left| \Delta \delta_{a,i} \right|$$
$$\overline{\delta_e} = \sum_{i=1}^{n} \left| \Delta \delta_{e,i} \right| \quad (8)$$

Table 3. Total aileron and elevator movement, represented in degrees traveled for various mission events and the entire mission length.

	Dive and roll initiation		Initiation of ascent		Entire mission	
	Fixed	Flexible	Fixed	Flexible	Fixed	Flexible
$\overline{\delta_a}$ (°)	144.22	176.06 (+ 22%)	162.23	258.51 (+ 59%)	408.14	538.54 (+ 32%)
$\overline{\delta_e}$ (°)	46.1	52.71 (+ 14%)	72.3	78.64 (+ 8.8%)	150.86	162.71 (+ 7.9%)

Agreeing with observations made during the pitch doublet, the greatest effect of dihedral deflection is seen in the lateral channels. Aileron activity for the flexible-wing configuration ranges from 22% to 59% more whereas elevator activity only ranges from 8.8% to 14% more. These percentages pertain to mission points B and D. Also noted during the simulation run was the maximum transient motion in angle-of-attack, sideslip, pitch, and roll for mission points B and D. Angle-of-attack, sideslip, and pitch transients did not differ significantly during both mission points. On the other hand, the maximum amplitude in roll angle transients during the dive / roll initiation was 6.76° for fixed-wing and 12.09° for flexible-wing, yielding a 79% increase in transient motion for the flexible-wing configuration.

C. Dihedral Step Response

Considering the observations made regarding the vehicle response, the question arose as to whether differences seen between the fixed and flexible-wing MAVs were driven by the stepwise change in dihedral, i.e. the discontinuity in the aerodynamics and mass properties. Tackling the above inquiry, a couple of maneuvers were considered: 1) dihedral doublets from non-trimmed conditions, and 2) a series of fixed-wing pitch doublets at various dihedral angles. Of interest in both of these tests is the magnitude of the transient motion in regard to that observed during the pitch doublet in section III-B.

The first set of maneuvers, the dihedral doublets, involved commanding two separate elevator deflections, each followed by a dihedral doublet. The doublets span from 7° to -5°, -5° to 30°, and back to 7°. General setup and execution of the dihedral doublets is shown in Figure 19. This maneuver was carried out twice, once with negative elevator deflections and once with positive (refer to mission points C1,C2 and D1,D2).

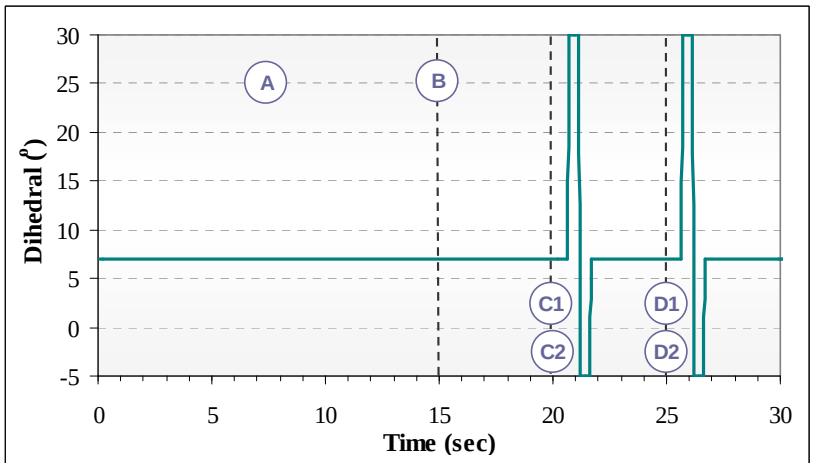

Figure 19. Dihedral doublets commanded after elevator step inputs.

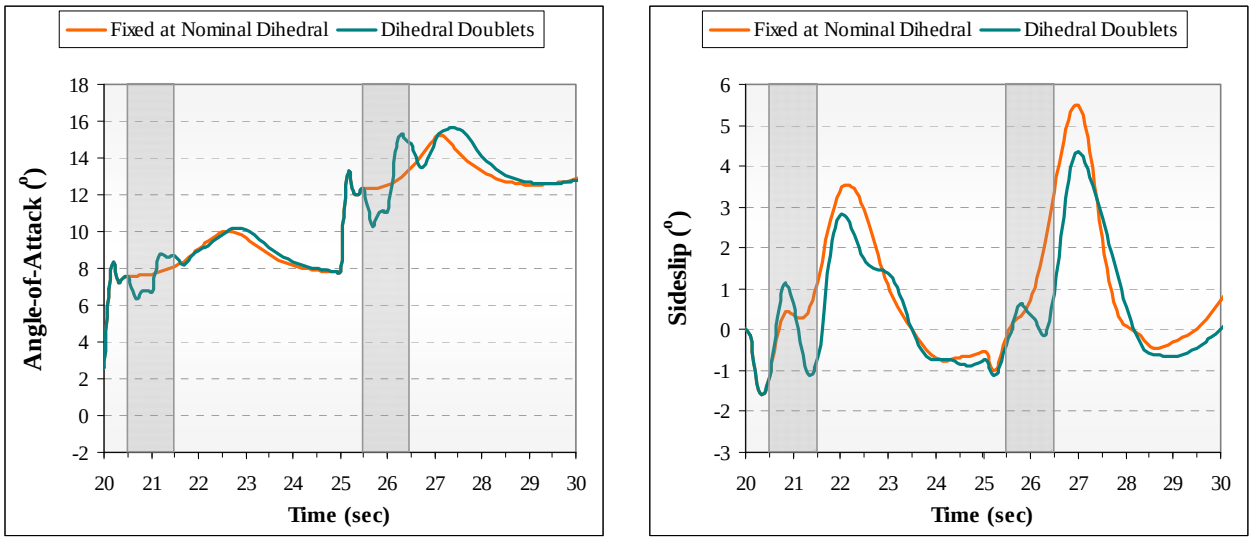

Figure 20. Angle-of-attack and sideslip motion induced by the dihedral doublets (marked by the shaded areas). This particular set of data corresponds to negative elevator deflections.

Beginning with angle-of-attack in Figure 20, it is clear where a dihedral change takes place based on the sudden jump in values, i.e. the discontinuity in aerodynamics and mass properties. This is much like the response observed with the sudden change in elevator deflection, though smaller in magnitude. Similar discontinuous behavior is observed in sideslip. Whether such jumps greatly impact the response of the flexible-wing to a pitch doublet is uncertain.

In Figure 21, the fixed-wing response to a pitch doublet for various dihedral angles is presented. The magnitude of response for all dihedral angles is large, similar to that seen in Figure 15 and Figure 17. It is possible the effects of the elevator deflections during a pitch doublet mask the discontinuity effects associated with dihedral step changes. For future studies, it would be best to smooth out discontinuities by interpolating the aerodynamic coefficients based on dihedral angle.

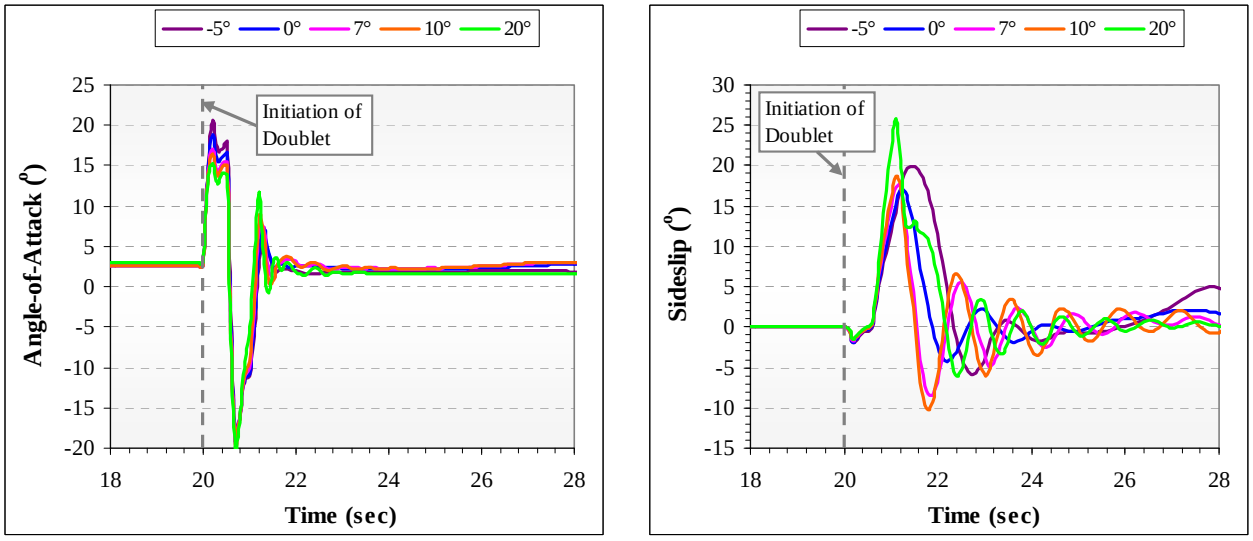

Figure 21. Angle-of-attack and sideslip response versus time resulting from a pitch doublet at various dihedral angles.

IV. Conclusions

In this paper, the effects of structural flexibility were studied on the flight mechanics of a micro aerial vehicle. This flexibility is a form of "passive morphing" that allows the airframe to deform due to aero-loading. Such deformations may be desirable for agile vehicle performance. A first-approximation simulation was developed that would allow for modification of the vehicle's aerodynamics and mass properties in response to such loading.

Referring back to section III-A, the amount of dihedral change due to vertical loading was arbitrarily chosen. Naturally, this is not a realistic representation. An improvement would be to model the wing deflection using beam theory, based upon the physical properties of the wing. Another approach would be the approximation of the wing as a series of mass-spring-damper systems. In either case, introducing curvature to the wings will not be a deterrent in predicting the aerodynamic coefficients, since AVL can handle such geometry.

For all of the simulation runs, no wind gust effects were included. It is well understood that wind gusts will play a big role in the control of MAVs during flight. This would be another helpful addition to the simulation. Wind gusts would change the dihedral of a flexible wing while disrupting the air vehicle from its flight path, possibly requiring the controller to work even harder to keep the plane at the proper orientation and altitude. As seen herein, vehicle flexibility may serve to reduce the vehicle response to such gusts and allow the disturbance to damp out quicker.

The symmetric dihedral deflection fails to capture the effects of sudden roll or yaw maneuvers on a flexible wing MAV, in which the individual wings experience significantly different loading. Allowing the wings to deflect individually would help in studying the response resulting from lateral maneuvers and assessing sensitivity to wind gusts.

A stepwise change in the dihedral and the corresponding change in aerodynamics introduce sudden jumps in the response of the aircraft, albeit small in magnitude. Taking advantage of the fact that the aerodynamics do not change by a drastically large amount between one dihedral breakpoint and the next, it seems safe to linearly interpolate between sets of aerodynamic coefficients for dihedral values that fall between the six dihedral breakpoints. The same method can be applied in updating the inertia matrix for the new dihedral value.

IV. Future Work

The simulation, in its current state, does not capture the complete set of dynamics that characterize flexible wing MAVs. Recognizing that more work needs to be done; the authors of this paper propose making the above additions to the simulation to better capture the behavior induced by a changing dihedral, starting with the asymmetric wing deflection. Additionally, the effects of atmospheric turbulence need to be included in the model to understand its effect on the vehicle flight mechanics. Finally, autopilot control strategies will be investigated that can exploit the features of a flexible vehicle for increased aerodynamic agility.

References

[1] *Air Force Research Laboratory / Munitions Directorate*, 11 Oct 2005, http://www.mn.afrl.af.mil/.

[2] Mueller, T.J., "Fixed and Flapping Wing Aerodynamics for Micro Air Vehicle Applications," Progress in Astronautics and Aeronautics, vol. 195, AIAA, Reston, 2001.

[3] Etkin, B., "Dynamics of Atmospheric Flight," Dover Publications, 2005.

[4] Ifju, P., Jenkins, D., Ettinger, S., Lian, Y., Shyy, W., and Waszak, R.M., "Flexible-Wing-Based Micro Air Vehicles," AIAA Paper 2002-0705, Jan. 2002.

[5] Albertani, R., Stanford, B., Hubner, J. P., and Ifju, P., " Characterization of Flexible Wing MAV' s: Aeroelastic and Propulsion Effects on Flying Qualities," Presented at the AIAA Atmospheric Flight Mechanics Conference, San Francisco, CA, 2005.

[6] Zipfel, P. H., *Fundamentals of Six Degrees of Freedom Aerospace Simulation and Analysis in FORTRAN and C++*, CD-ROM, AIAA Self-Study Series, 2004.

[7] Zipfel, P. H., *Modeling and Simulation of Aerospace Vehicle Dynamics*, AIAA Education Series, 2000.

[8] *Athena Vortex Lattice*, 29 April 2006, Massachusetts Institute of Technology, http://web.mit.edu/drela/Public/web/avl/.

[9] DeLuca, A., Reeder, M., Freeman, J., and Ol, M., "Flexible- and Rigid- Wing Micro Air Vehicle: Lift and Drag Comparison," AIAA Journal of Aircraft, Vol. 43, No. 2, March-April 2006, pp. 572-575.

[10] *Low Observable Design Synthesis Tool*, May 1994, Air Force Research Laboratory / Information Systems Research, http://www.rl.af.mil/tech/papers/ModSim/DU94.html.

[11] Phillips, W. F., *Mechanics of Flight*, John Wiley & Sons, Inc., New Jersey, 2004.

[12] Brumbaugh, R.W., Aircraft Model for the AIAA Controls Design Challenge, Journal of Guidance, Control, and Dynamics, Vol. 17., No. 4, July – August, 1994.

[13] Nelson, R. C., *Flight Stability and Automatic Control*, 2nd Ed., The McGraw-Hill Companies, Inc., 1998.

Appendix 2

On Design of the Air Force Research Laboratory Micro Aerial Vehicle Research Configuration

This page intentionally left blank

Design of the Air Force Research Laboratory Micro Aerial Vehicle Research Configuration

Kelly Stewart[*], Jeffrey Wagener[†], and Gregg Abate[‡]
Air Force Research Laboratory Munitions Directorate, Eglin AFB, FL, USA

and

Max Salichon[§]
PhD student in Dynamics and Controls, Oregon State University, Corvallis, OR, USA

The Air Force Research Laboratory Munitions Directorate (AFRL/MN) is presently involved in many aspects of micro aerial vehicle (MAV) research. Among these are: advanced modeling and simulation models for MAVs, aero-structural interaction, advanced guidance techniques, digital simulations, and vehicle integration. In order to optimize collaboration within AFRL and also with outside research organizations, it was decided that a common MAV configuration be designed that would serve as a reference for current and future research. This paper describes a generic micro air vehicle that will serve as a "baseline" configuration. The MAV design incorporates a circular fuselage, a thin cambered wing, and a conventional tail. The MAV has a wingspan of 24 inches and a fuselage length of 17 inches. This paper will also detail the rational behind the design as well as provide initial aerodynamic properties and flight performance characteristics of the AFRL Generic MAV, herein called "GENMAV."

Nomenclature

ρ	=	air density
Γ	=	dihedral angle
ϕ, θ, ψ	=	Euler angles [roll, pitch, yaw]
b	=	wing span
c	=	chord
C_D	=	drag coefficient
C_L	=	lift coefficient
C_l	=	roll moment coefficient
$C_{l\alpha}$	=	roll moment versus angle-of-attack stability derivative
$C_{l\beta}$	=	roll moment versus sideslip angle stability derivative
C_{lp}	=	roll moment versus roll rate stability derivative
C_{lr}	=	roll moment versus yaw rate stability derivative
C_m	=	pitch moment coefficient
C_{mq}	=	pitch moment versus pitch rate stability derivative
$C_{m\alpha}$	=	pitch moment versus angle-of-attack stability derivative
C_{np}	=	yaw moment versus roll rate stability derivative
C_n	=	yaw moment coefficient
C_{nr}	=	yaw moment versus yaw rate stability derivative
$C_{n\beta}$	=	yaw moment versus sideslip angle stability derivative

[*] Member, AIAA (850 883 2633, kelly.stewart@eglin.af.mil)
[†] Member, AIAA
[‡] Associate Fellow AIAA
[§] Member AIAA

p, q, r	=	body rates [roll, pitch, yaw]
V	=	airspeed
x,y,z	=	coordinate axes in aircraft frame

I. Introduction

THE US Air Force Research Laboratory Munition Directorate (AFRL/MN)[1] is pursuing many avenues of research for micro aerial vehicles (MAV). Micro aerial vehicles (MAV) are characterized by small vehicle size ($\mathcal{O}$ 10 cm), low flight speeds ($\mathcal{O}$ 10 m/s), and low Reynolds number ($\mathcal{O}$ 10,000-100,000). The desire to develop MAVs is fueled by the need for increased situational awareness (especially in urban environments), remote sensing capability, "over the hill" reconnaissance, precision payload delivery, and aid in rescue missions. Figure 1 depicts where MAVs lay on the mass versus Reynolds number plot for flight vehicles and Figure 2 depicts some examples of MAVs. MAVs can be considered a sub-class of uninhabited air vehicles (UAVs). UAVs have been developed in recent years by leveraging traditional aerospace science technologies. However, the engineering maturity required for MAV development has not kept pace. For instance, due to the extremely small size of MAVs, the flowfield is dominated by separated flow regimes on the order of the vehicle size. Also, the small size of MAVs gives rise to small inertias which make the MAV more susceptible to wind gusts.

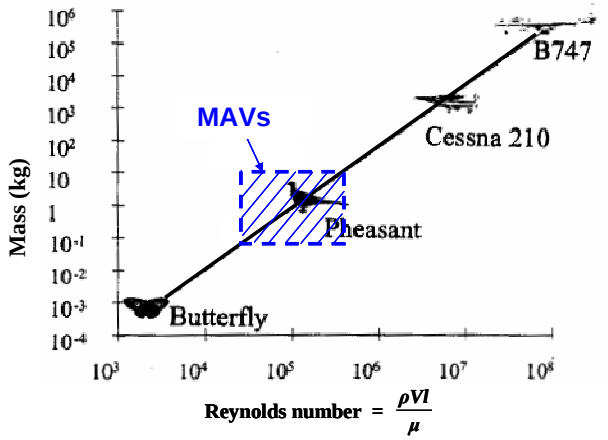

Figure 1. Mass versus Reynolds number for MAVs[2]

Figure 2. Examples of MAVs

In recent years, interest and development of micro aerial vehicles has been greatly increased. As such, many concepts and designs have emerged for MAVs. However, if one wants to study only certain aspects of MAVs, such as an advanced aerodynamic wing or advanced guidance, navigation, and control (GNC) methodologies, the various designs do not lend themselves well for trade studies. This need has led AFRL/MN to propose a "baseline" geometry for a MAV that can be openly distributed amongst various organizations for easy comparison of concepts and technologies. The aim of this paper is to describe in detail the geometry of the USAF Generic MAV, herein called "GENMAV," as well as providing initial aerodynamic prediction data as determined from a vortex-panel code.

II. The GENMAV Design

Design of the US Air Force Research Laboratory Generic Micro Air Vehicle, or "GENMAV," is loosely fashioned after similar MAV designs that have been studied in the past[3] and which are shown in Figure 3. Here are seen two micro air vehicles with 24" wingspans and 6" chords. These vehicles are designed for a flight speed between 10 and 50 mph which results in chord-Reynolds numbers from 50,000 – 250,000. This Reynolds number regime is characterized as "low" in the fixed-wing aircraft community where flow separation is of concern[4,5]. The designs depicted in Figure 3 also use a "V-tail" configuration and have a fuselage design that is not very well detailed in the literature. Additionally, details about the airfoil section were not very well defined.

It was decided that a standard, generic MAV configuration be defined that would serve as a reference for all future MAV studies. This MAV would be termed "GENMAV". GENMAV would be of similar size to the vehicles studied in Reference 3 but would employ simple conventional designs. Future MAV studies could begin with GENMAV as a starting point for design spirals and the resulting performance data would be referenced to a common design.

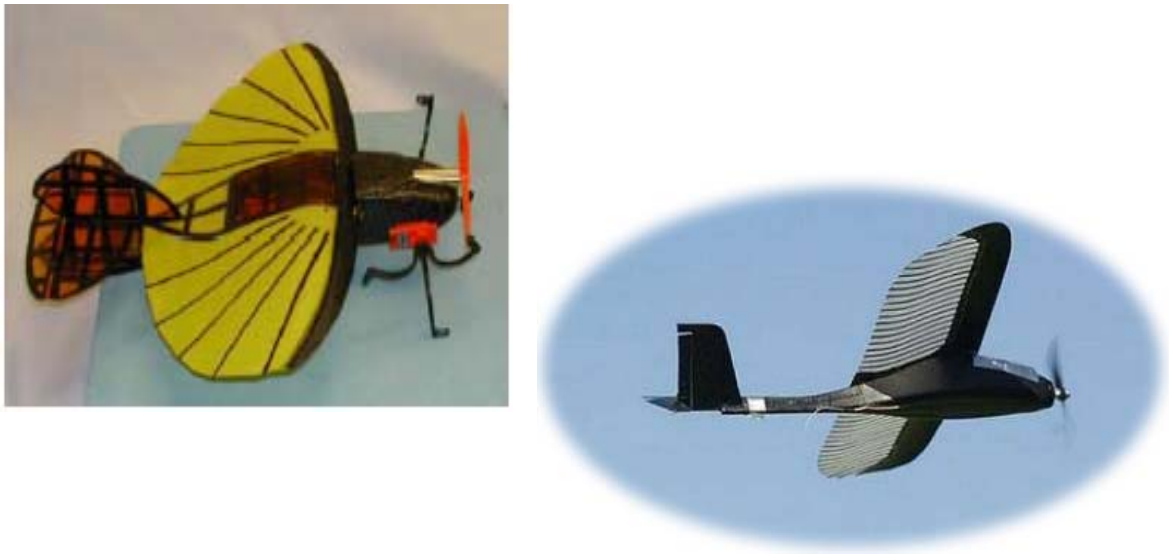

Figure 3. Previous MAV designs studied that provided inspiration for a generic MAV design.

A. GENMAV Layout

GENMAV is a high-wing aircraft configuration with a circular fuselage and a conventional tail. GENMAV is depicted in Figure 4. Here it is seen that the vehicle is similar to a conventional aircraft design. Note that there is a "saddle" structure that is designed to smoothly transition the wing to the circular fuselage. Also note that the wings have a positive dihedral. While no engine or propeller is depicted in Figure 4, a tractor propeller is located at the front of the vehicle. However, no details about the propeller and engine will be defined at this point in the development.

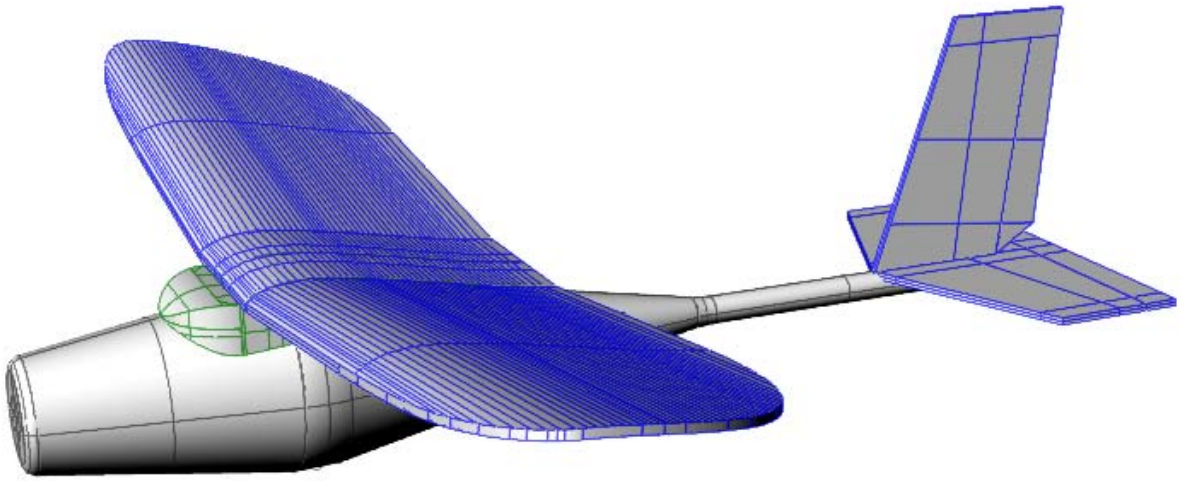

Figure 4. GENMAV configuration.

B. Fuselage

As mentioned, the GENMAV has a circular fuselage. The main reason for selecting a circular fuselage was for ease in aerodynamic analysis. However, the circular cross-section fuselage may be slightly more difficult to manufacture depending upon the construction method and it will be more difficult to place internal components. But it was felt that a circular design would provide a better baseline design. Figure 5 shows the side view of GENMAV where the fuselage shape is clearly seen. Note here the wing saddle which provides a transition between the wing and the fuselage. Additionally, this saddle allows for easy setting of the wing incidence angle which has been initially set to 5 degrees.

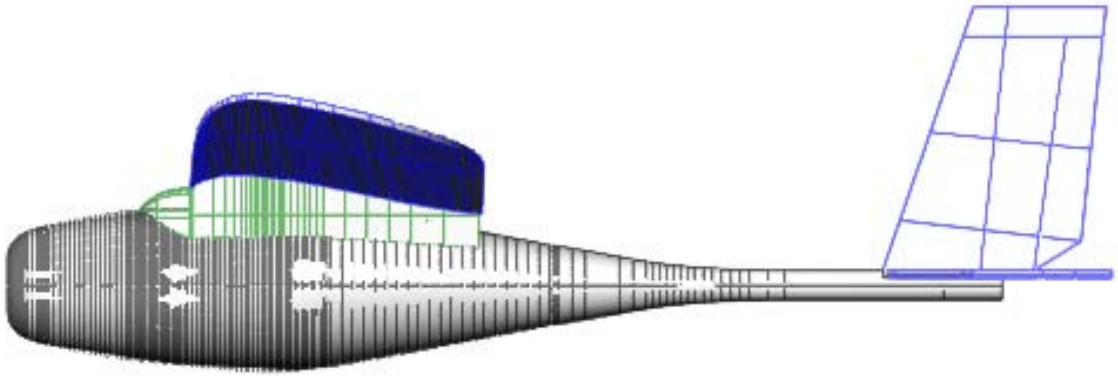

Figure 5. GENMAV side view showing fuselage design.

C. Wing

The GENMAV wing is a thin airfoil configuration with positive dihedral of 7 degrees. The root chord is 5" and the span is 24". The GENMAV wing is less elliptical in planform than that of the MAVs in Reference 3. This was due to poor low speed performance attributed to tip-stall noted in flight testing of the MAVs of Reference 3. Because of this, a planform geometry was developed[6] in which the chord distribution is given by the expression

$$c(y) = C_r \sqrt{1 - \left(\frac{2|y|}{b} \right)^{\tau}} \ , \ y = \left(-\frac{b}{2}, \frac{b}{2} \right). \tag{1}$$

Here, y is the spanwise coordinate, C_r the root chord, b the wing span, and τ = 8. This does not result in a rectangular wing, but rather a wing with a fairly constant chord for most of the span, with a rounded tip, as shown in Figure 6.

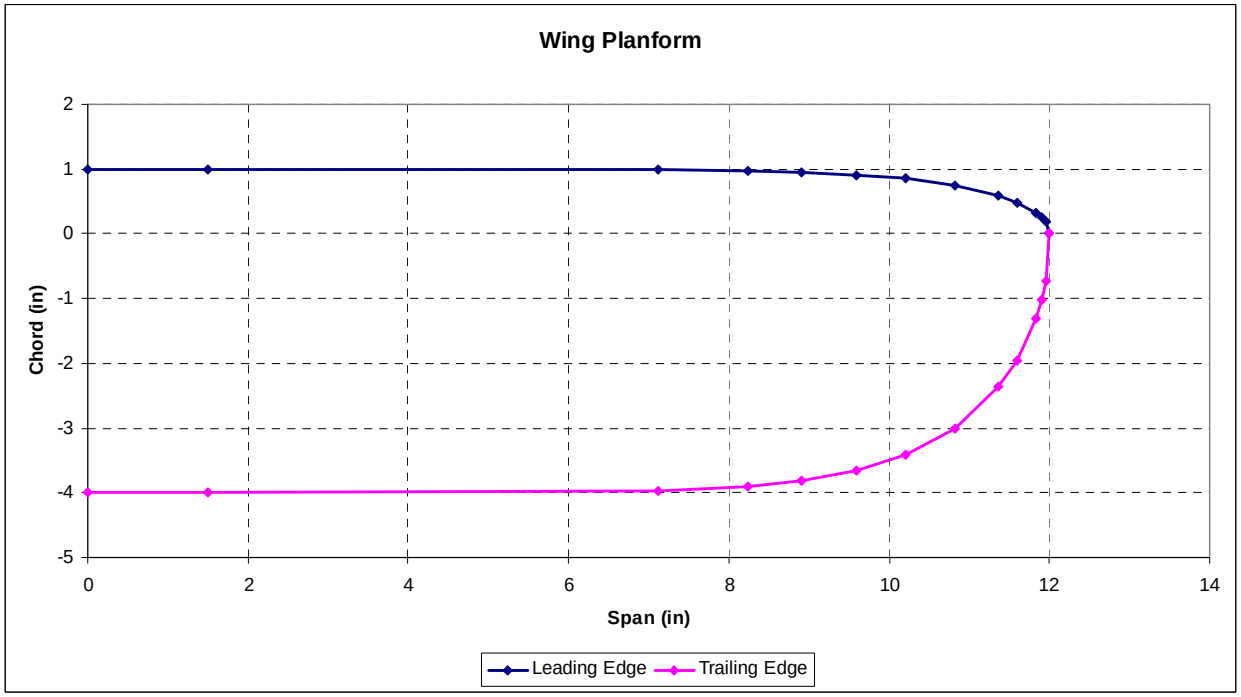

Figure 6. GENMAV wing planform.

The GENMAV airfoil shape is based upon a design from the University of Florida[7] as were the MAV designs of Reference 3. This airfoil did have some reflex incorporated into it as it was originally designed for a tail-less MAV concept. However, a rigorous redesign of the airfoil was not possible so it was decided to remove as much of the reflex beyond 30% of the chord length (x/c). The resultant airfoil is depicted in Figure 7 and the GENMAV airfoil coordinates are given in Table 1. Note that this airfoil shape is constant the entire span of the wing and that the curved tips are a simple cut-out from this constant chord.

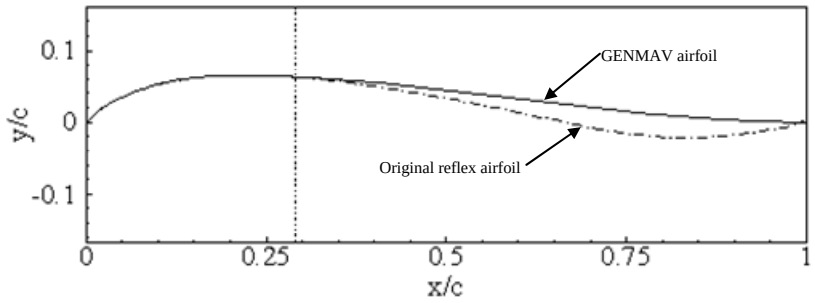

Figure 7. GENMAV airfoil section.

D. Empennage

Conventional horizontal and vertical stabilizers were chosen for the GENMAV tail assembly. This was done to allow for a more conventional analysis of the GENMAV as well as alleviate any issues associated with a V-Tail. Many aeroprediction methods and simulations are based upon rudder and elevator commands so having a more conventional tail made the most sense. The rudder and elevator are approximately 25% of the tip chord for each stabilizer and run parallel with the trailing edge.

E. Engine

No engine or propeller is presently sized for GENMAV. It is anticipated that the engine will be aligned with the centerline of the fuselage and have an appropriately sized propeller disk.

F. GENMAV Dimensions

Figure 8 depicts the final GENMAV layout with dimensions. All dimensions are in inches. The center of gravity is located 4.15" behind the nose of the GENMAV and is vertically offset above the fuselage centerline by 0.58". Note also that there is no wing dihedral for the first 1.5" of wing semi-span and then the dihedral is a constant 7 degrees. The vertical and horizontal stabilizers both start at 14.96" behind the nose of the GENMAV. The wing incidence angle is set to 5 degrees. The fuselage diameter is slightly larger than 3" at its widest point.

Table 1. GENMAV airfoil coordinates

x/c	y/c
0.00000	0.00000
0.01429	0.01256
0.02857	0.02241
0.04361	0.03120
0.06019	0.03928
0.07677	0.04586
0.09394	0.05132
0.11143	0.05566
0.12893	0.05895
0.14677	0.06140
0.16462	0.06308
0.18250	0.06412
0.20046	0.06465
0.21842	0.06474
0.23637	0.06448
0.25433	0.06394
0.27229	0.06318
0.29020	0.06225
0.30810	0.06117
0.32599	0.05998
0.34383	0.05869
0.36167	0.05733
0.37948	0.05590
0.39725	0.05440
0.41503	0.05285
0.43276	0.05124
0.45048	0.04958
0.46820	0.04785
0.48588	0.04607
0.50356	0.04423
0.52122	0.04233
0.53888	0.04037
0.55653	0.03836
0.57415	0.03630
0.59177	0.03421
0.60938	0.03208
0.62695	0.02993
0.64452	0.02777
0.66210	0.02562
0.67970	0.02348
0.69729	0.02137
0.71498	0.01931
0.73271	0.01731
0.75044	0.01539
0.76827	0.01356
0.78616	0.01185
0.80409	0.01026
0.82205	0.00881
0.84002	0.00751
0.85797	0.00635
0.87591	0.00533
0.89381	0.00444
0.91166	0.00365
0.92947	0.00292
0.94721	0.00222
0.96489	0.00149
0.98248	0.00065
1.00000	0.00000

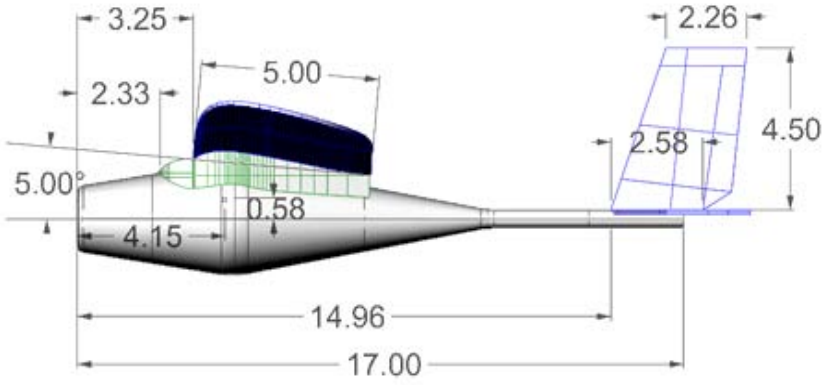

a) side view

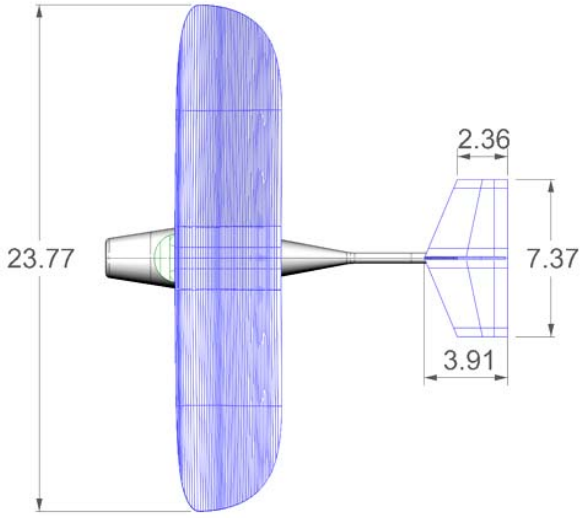

b) top view

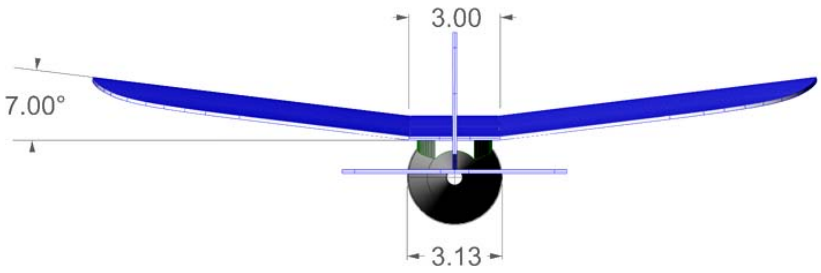

c) rear view

Figure 8. GENMAV dimensioned layout.

III. Aerodynamic Characteristics

An initial estimate of the aerodynamic characteristics of the GENMAV has been obtained through the Athena Vortex Lattice (AVL)[8] aeroprediction code, which is a vortex-lattice method. The flight regime of the vehicle ranges from about Mach 0.02 (15 mi/hr) to Mach 0.06 (45 mi/hr) at sea level conditions. Within this range, the aerodynamics do not change much and are mostly a function of angle-of-attack. AVL considers only the wing and tail surfaces to predict the vehicle aerodynamics. No contribution from the fuselage is considered. Hence, a drag correction must be added to the AVL results. A base drag correction of 0.06 was added to the drag data. This value was estimated from zero-yaw drag data given in Reference 3.

A. Lift and Drag data

Figure 9a shows the lift coefficient as a function of angle-of-attack for various side-slip angles and Figure 9b shows the lift coefficient vs. angle-of-attack for various elevator deflections. As AVL is a vortex-lattice code, flow separations are not predicted and therefore the lift data is fairly linear and does not show a stall angle. In the wind tunnel data of Reference 3, stall was seen at 8-10 degrees angle-of-attack.

Figure 10a depicts the drag data as predicted for GENMAV by AVL as a function of angle-of-attack versus side-slip angles and Figure 10b shows the same data for various elevator deflections. Note that the zero-yaw drag value of 0.06 is added to the drag data by AVL to account for the friction drag of the fuselage. Similarly, the lift-drag ratio versus angle of attack is given in Figure 11.

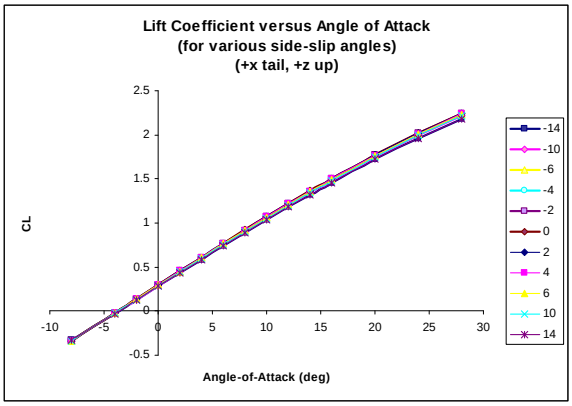

a) C_L vs. Angle-of-attack for various side-slip angles

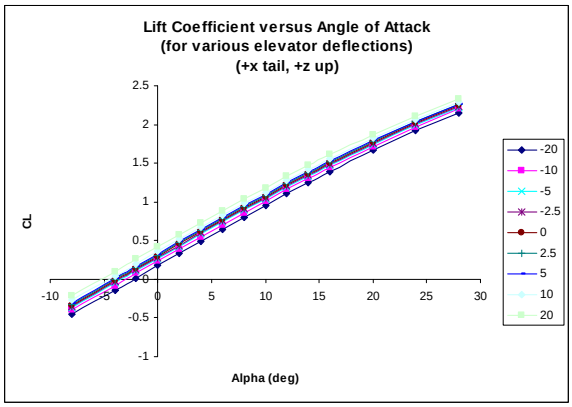

b) C_L vs. Angle-of-attack for various elevator deflections

Figure 9. GENMAV aerodynamic lift data.

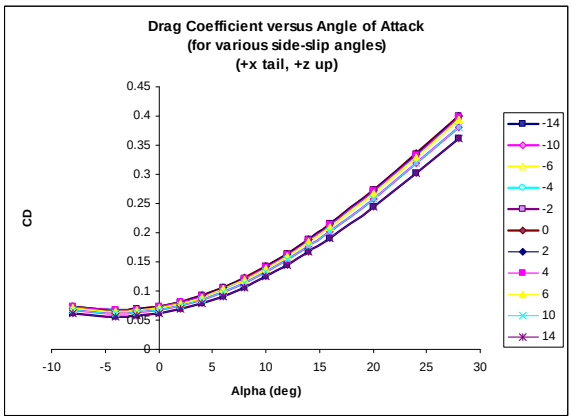

a) C_D vs. Angle-of-attack for various side-slip angles

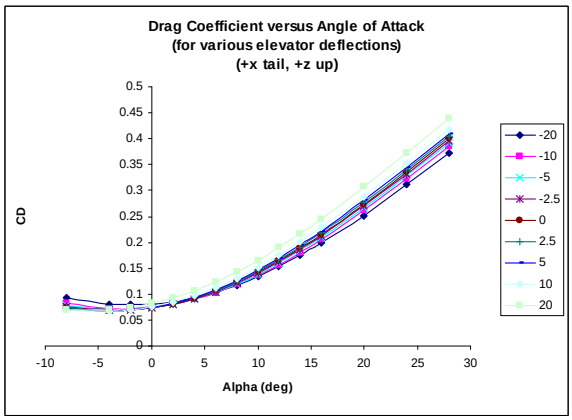

b) C_D vs. Angle-of-attack for various elevator deflections

Figure 10. GENMAV aerodynamic drag data.

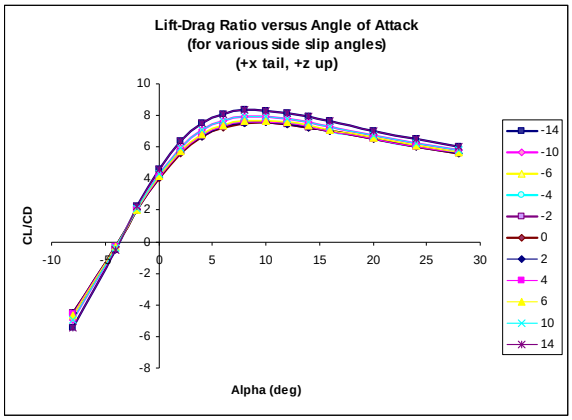

a) C_L/C_D vs. Angle-of-attack for various side-slip angles

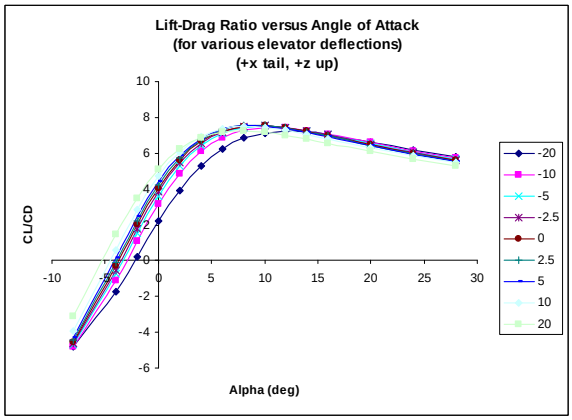

b) C_L/C_D vs. Angle-of-attack for various elevator deflections

Figure 11. GENMAV lift-drag data versus angle-of-attack.

B. Moment Data

The aerodynamic moment data in roll, pitch, and yaw are also calculated by AVL. Figure 12 shows the roll moment coefficient as a function of angle of attack for various side-slip angles as well as the roll moment coefficient as a function of rudder deflection for various angles of attack. Figure 13 shows the pitch moment coefficient variation as a function of angle of attack for various side-slip angles as well as the change in pitch moment for various elevator deflections at various angles of attack. Finally, Figure 14 shows similar changes of the yaw moment coefficient with angle of attack and rudder deflections.

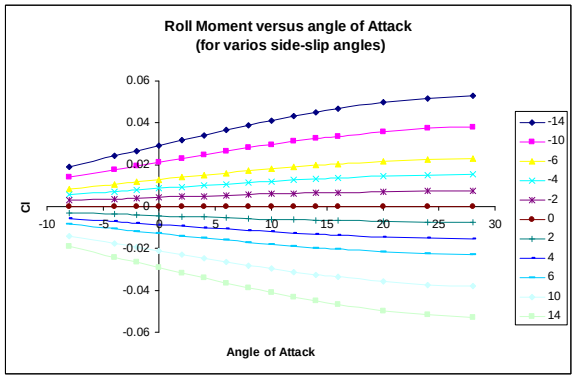

a) C_l vs. Angle-of-attack for various side-slip angles

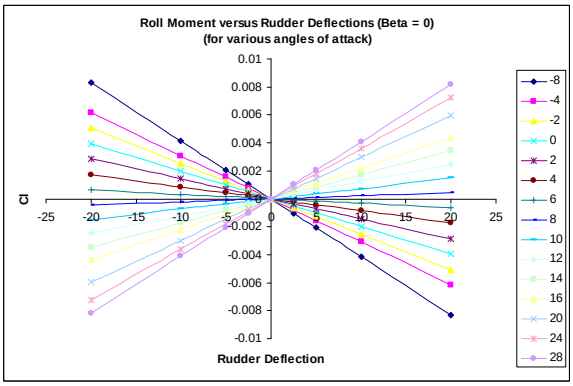

b) C_l vs. Angle-of-attack for various rudder deflections

Figure 12. GENMAV roll moment data.

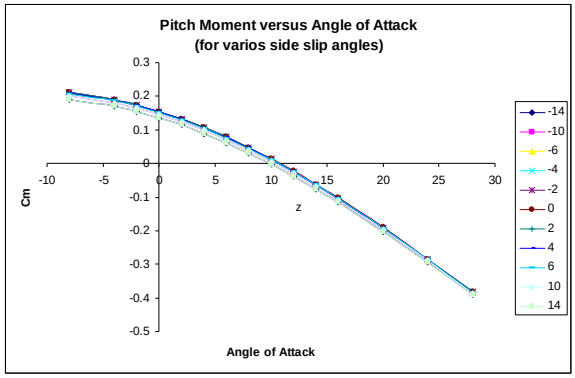

a) C_m vs. Angle-of-attack for various side-slip angles

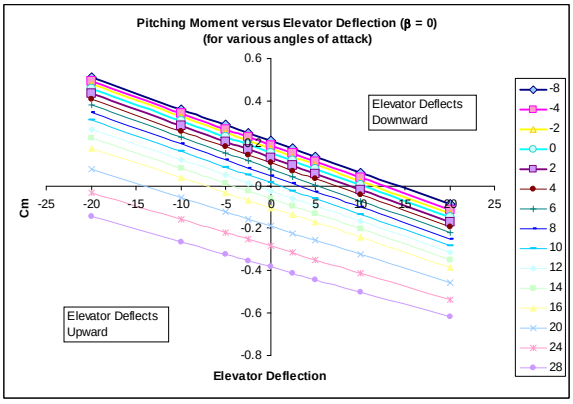

b) C_m vs. Angle-of-attack for various elevator deflections

Figure 13. GENMAV pitch moment data.

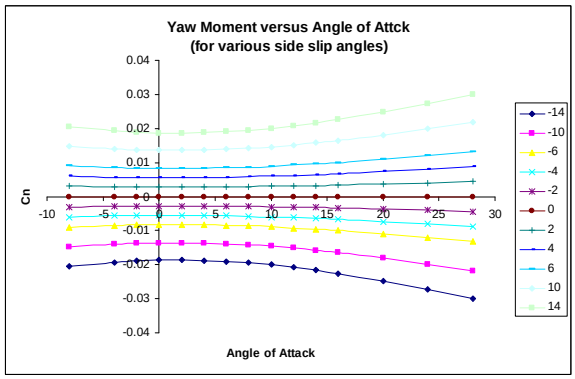

a) C_n vs. Angle-of-attack for various side-slip angles

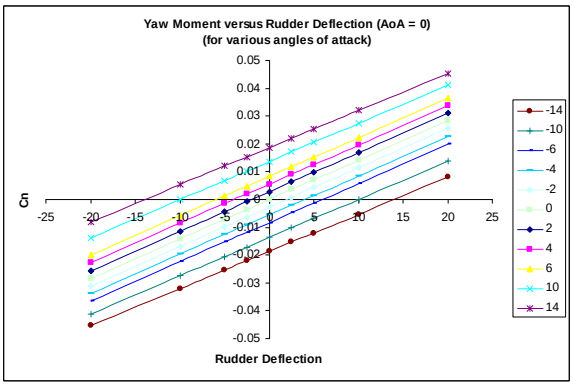

b) C_n vs. Angle-of-attack for various rudder deflections

Figure 14. GENMAV yaw moment data.

C. Stability Derivatives

A summary of the stability derivatives as determined by AVL for the GENMAV configuration at a standard cruising speed of 30 mph is given in Table 2. Here it is seen that the airframe is stable in all three axes. Note also that the airframe exhibits very good spiral stability based on the relation ($C_{l\beta}C_{nr} / C_{n\beta}C_{lr}$) > 1 (in fact, $C_{l\beta}C_{nr} / C_{n\beta}C_{lr}$ equals 12.0).

Table 2. GENMAV Stability derivatives

$C_{l\beta}$	C_{lp}	C_{lr}	$C_{m\alpha}$	C_{mq}	$C_{n\beta}$	C_{np}	C_{nr}
-0.162	-0.496	0.191	-1.45	-12.5	0.005	-0.040	-0.071

IV. Prototyping

A first prototype of the GENMAV was recently completed. This was accomplished at a micro air vehicle fabrication laboratory. A 3-D printer was used to "print" the fuselage and wing molds. Figure 15 depicts the fuselage sections and saddle piece as well as the wing mold that were used for prototyping. With the completed fuselage mold, carbon-fiber cloth is used to wrap the mold. For the wing, a carbon-fiber cloth is used in the wing mold and is vacuum-sealed during the curing process. The finished wing conforms to the shape of the mold. The final planform of the wing is cut after the wing is dry. Flat carbon-fiber panels are used for the empennage section.

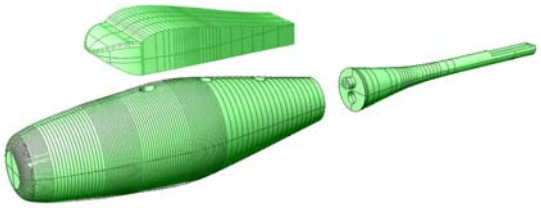

Fuselage & Saddle piece

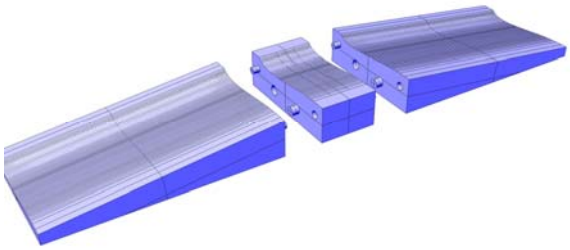

Wing mold

Figure 15. GENMAV Component CAD files for 3D printing.

Figure 16 shows the completed GENMAV prototype which was recently installed in the Oregon State University low speed wind tunnel. Unfortunately, data analysis was not possible before the publication of this paper.

Figure 16. Prototype GENMAV in Oregon State University Wind Tunnel.

V. Conclusions and Future work

This paper outlines the geometric properties of the AFRL Baseline Generic MAV (GENMAV) configuration. Aerodynamic analysis was performed on this configuration with the Athena Vortex Lattice (AVL) aeroprediction code. The AVL code gave reasonable approximations to the GENMAV aerodynamics. GENMAV provides the aerospace community a common starting ground: a conventional, stable airframe from which different MAV technologies and trade studies can be applied. It is hoped this basic framework will aid the research community by allowing a true comparison to be made between modifications applied by various organizations.

Future work will include more aerodynamic analysis through wind tunnel testing (presently underway) as well as computationally. The prototype GENMAV will also undergo flight tests as well in which flight data will be recorded and analyzed. These tests include defining the maximum / minimum airspeed and observing the vehicle's handling qualities in roll, pitch, and yaw. Once familiarization with the air vehicle is complete, further flight testing can take place to document the flying qualities of the baseline MAV configuration. Data from these flight tests will act as the control point to which modified versions of the MAV can be compared. Flight test data can also be used to validate a 6-degree-of-freedom (6-DOF) simulation currently under development. It is hoped other organizations will adopt the GENMAV configuration and perform analysis on it as well to further increase the understanding of the configuration.

References

[1] http://www.mn.afrl.af.mil/

[2] Mueller, T.J., "Fixed and Flapping Wing Aerodynamics for Micro Air Vehicle Applications," Progress in Astronautics and Aeronautics, vol. 195, AIAA, Reston, 2001.

[3] DeLuca, A., Reeder, M., Ol, M., Freeman, J., Bautista, I., and Simonich M., "Experimental Investigation into the Aerodynamic Properties of a Flexible and Rigid Wing Micro Air Vehicle," AIAA Paper 2004-2396, June 2004.

[4] Ifju, P., Jenkins, D., Ettinger, S., Lian, Y., Shyy, W., and Waszak, R.M., "Flexible-Wing-Based Micro Air Vehicles," AIAA Paper 2002-0705, Jan. 2002.

[5] Carmichael, B.H. "Low Reynolds Number Airfoil Survey, Vol. 1". NASA CR 165803, November 1981.

[6] Deryl Snyder, *personal communication*

[7] Nechyba, M., and Ifju, P. "Towards Autonomous Flight of Micro Air Vehicles (MAVs): Vision-Guided Flight Stability and Control," Informational Briefing-Audience Unknown, Department of Electrical and Computer Engineering and Department of Aerospace and Mechanical Science, University of Florida, Gainesville Florida, 2002.

[8] http://web.mit.edu/drela/Public/web/avl/

Appendix 3

Development and Initial Flight Tests of a Single-Jointed Articulated-Wing Micro Air Vehicle

This page intentionally left blank

Development and Initial Flight Tests of a Single-Jointed Articulated-Wing Micro Air Vehicle

Kelly C. Stewart[*], Ken Blackburn[†], Jeffrey Wagener[‡], Lt. Joseph Czabaranek[§], and Gregg Abate[**]
Air Force Research Laboratory - Munitions Directorate, Eglin AFB, FL, USA

A prototype of an articulated-wing micro air vehicle (MAV) has been developed at the Air Force Research Laboratory Munitions Directorate (AFRL/RW) with the purpose of studying passive wing deformation in response to wind gusts. The prototype is a first iteration towards a final design meant to provide insight into the flight and control of MAVs in gusty environments. This paper details the design of two MAVs, one of which is a fixed-wing baseline configuration, and one of which is the articulated-wing prototype. The baseline configuration will act as the reference point to which the flight characteristics of the articulated-wing prototype can be compared. Coinciding with the prototype is a digital simulation that will model the flight characteristics of the MAV and act as a stepping stone for more complex simulations involving multi-jointed wing MAVs.

Nomenclature

C_x	=	axial force coefficient
$C_{x\alpha}$	=	axial force versus angle-of-attack stability derivative
C_{xq}	=	axial force versus pitch rate stability derivative
C_y	=	side force coefficient
$C_{y\beta}$	=	side force versus sideslip angle stability derivative
C_{yp}	=	side force versus roll rate stability derivative
C_{yr}	=	side force versus yaw rate stability derivative
C_z	=	normal force coefficient
$C_{z\alpha}$	=	normal force versus angle-of-attack stability derivative
C_{zq}	=	normal force versus pitch rate stability derivative
C_l	=	roll moment coefficient
$C_{l\beta}$	=	roll moment versus sideslip angle stability derivative
C_{lp}	=	roll moment versus roll rate stability derivative
C_{lr}	=	roll moment versus yaw rate stability derivative
C_m	=	pitch moment coefficient
$C_{m\alpha}$	=	pitch moment versus angle-of-attack stability derivative
C_{mq}	=	pitch moment versus pitch rate stability derivative
C_n	=	yaw moment coefficient
$C_{n\beta}$	=	yaw moment versus sideslip angle stability derivative
C_{np}	=	yaw moment versus roll rate stability derivative
C_{nr}	=	yaw moment versus yaw rate stability derivative

I. Introduction

THE Air Force Research Laboratory has a keen interest in the development of micro air vehicles (MAVs) for use in military applications such as reconnaissance, situational awareness, precision payload delivery, and aid in rescue. While the smaller size of MAVs makes them ideal for easy transportation and flight in urban environments,

[*] Aerospace Engineer, AFRL/RWGN, 101 West Eglin Blvd, Eglin AFB FL, 32542, Senior Member.
[†] Product/Project Engineer, AFRL/RWAV, 101 West Eglin Blvd, Eglin AFB FL, 32542, Senior Member.
[‡] Mechanical Engineer, AFRL/RWAV, 101 West Eglin Blvd, Eglin AFB FL, 32542.
[§] Mechanical Engineer, AFRL/RWAV, 101 West Eglin Blvd, Eglin AFB FL, 32542.
[**] Aerospace Engineer, AFRL/RWGN, 101 West Eglin Blvd, Eglin AFB FL, 32542, Associate Fellow.

the smaller size also carries a new set of problems in regards to flight mechanics and control. The MAV flight mechanics challenge consists of generating sufficient control power to maneuver, to negotiate gusts while keeping sensors on target, to remain controllable in ground effects or presence of other obstacles, to precisely maintain path and orientation in confined spaces, to "perch" and perform related maneuvers of precision landing, and to achieve all of these with minimal onboard energy, with low resolution air data sensors and with limited onboard computational resources[1]. Of these challenges, increased susceptibility to wind gusts, in part due to the small inertias of the MAV, remains an active area of research.

One approach to gust alleviation for MAVs is to use adaptive washout[2], that is, to allow the wings to passively deform in response to wind gusts. This concept is used in many existing aircraft designs. Here, the bending of the wing during adaptive washout counters the effect of the aerodynamic loads generated by the gust, thus, minimizing the disturbance. Another strategy for achieving gust tolerance involves "biological inspiration," that is, understanding from natural fliers (e.g., bats, birds, insects, etc.) how they compensate for gusts and using such features in MAVs. One example is exploiting "flexible" structures. Such structures deflect to absorb gust energy and admit actuation at resonant frequency, thus reducing flight power requirements.

Structural flexibility implies that part of the MAV structure (or parts of the structure) has a certain amount of designed flexibility which lends itself to deformations favorable to gust alleviation. An example of this structural flexibility in nature is the small-scale shape changes that result from a bird's feathers bending that allow a bird to reject a gust or fly at high angles of attack (note that this is different from a bird being able to fold its wing which is considered morphing). This concept is best exemplified by pilots of radio-controlled MAVs that report MAVs with a "flexible" wing (i.e., covered in a latex material) are easier to fly than MAVs with a rigid wing[3]. It is reasonable to assume that for a MAV with a flexible wing, gust energy would be, to some extent, absorbed by the flexibility of the structure. This absorption of the energy (and subsequent dissipation) would reduce the amount of energy that goes into disturbing the vehicle thereby reducing the impact of the gust. Additionally, Breuer, et al.[4] and Gursul et al.[5], have shown that airfoils which are compliant delay stall and reduce the separation region.

Presented in this paper is a MAV prototype that uses an articulated-wing to allow for passive deformation. The prototype is a modification of a fixed-wing design that serves as a "baseline" configuration for on-going MAV research[6]. This same wing that is able to deform during wind gusts will also deform during rapid flight maneuvers, which can be expected of MAVs flying in tightly confined environments. Coinciding with this prototype is a digital simulation that allows for the exploration of varying degrees of wing articulation. A study of one vehicle, whose wings were rigid but the dihedral was allowed to change according to the aerodynamic loads, showed that the response of an aircraft could possibly be improved[7]. The reason for exploring an articulated-wing MAV versus a flexible-wing was ease of modeling. While experimentally testing an MAV with flexible wings is feasible, the computational modeling of the wing deformation is far more involved, usually requiring some sort of FEM analysis. Rather, it was desired to have a model that provides a good approximation of a flexible wing, but executes quickly enough to operate in a simulated mission. To this end, an articulated-wing prototype has been developed for experimental testing and will be the same vehicle modeled in the digital simulation.

II. Baseline Configuration

Prior to the development of an articulated-wing MAV, it was realized that a baseline design would be needed to act as a starting reference point for any future prototype development. This led to the definition of a rigid, fixed-wing configuration that follows a conventional aircraft design. The configuration is loosely based on existing MAV designs that have been studied previously[8]. By having a reference vehicle, any modifications made with the intent of exploring various MAV technologies can be compared back to the "baseline" and their effect better understood. Throughout this paper, the baseline configuration will be referred to as "GenMAV 1".

A. GenMAV 1 Layout

GenMAV 1 uses a high-wing configuration with a wingspan of 24" and a chord of 5". It has a conventional tail with a horizontal surface of 12" and a vertical surface of 4.6". The fuselage is 16.5" in length and approximately 3" in diameter at its widest point. GenMAV 1 is a bank-to-turn vehicle controlled by a pair of elevons that make up 50% of the chord on the horizontal stabilizer. The vertical and horizontal stabilizers were manufactured out of three plies of 0/90 woven carbon fiber. The vertical stabilizer was constructed in a [30, 120/0, 90/30, 120] layup in a crude attempt to limit torsion due to sideslip. Existing materials and molds from the MAV lab at AFRL were used for the wing and fuselage. The wing was constructed of up to three plies of woven carbon fiber / epoxy at the leading edge, tapering to one ply [+-45] at the trailing edge. The body of the vehicle is constructed of carbon fiber with enough

layers used in the wings to ensure adequate rigidity. Shown below in Figure 1 are photographs of a completed GenMAV 1 ready for flight.

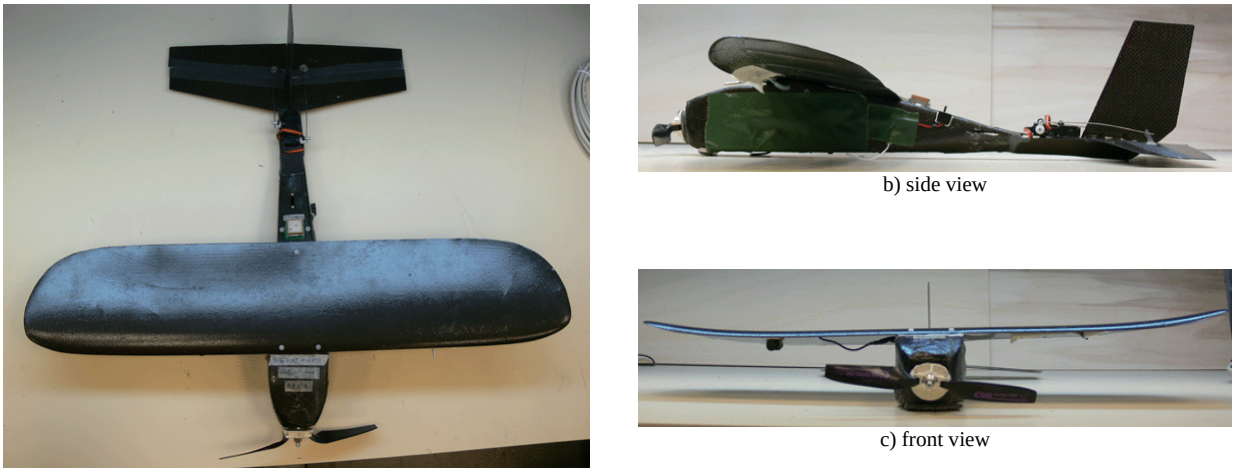

a) top view

b) side view

c) front view

Figure 1. Flight-ready GenMAV 1.

GenMAV1 is equipped with a Kestrel 2.2 autopilot for autonomous flight capability. The autopilot subsystem includes a radio transceiver for sending commands and receiving telemetry, and a GPS antenna for position information. The autopilot provides sensor data (accelerations, rotation rates, total and static pressure), 2 Hz telemetry data for the entire flight, and selectable data rates for up to 100 time steps. A data rate of 20 Hz over a 5-second window was used during flight test maneuvers to allow characterization of flight modes. The autopilot system also aids in takeoff, landing, and stabilization of the aircraft before test maneuvers. The flight maneuvers are flown open loop to allow aircraft motion to reflect fixed surface dynamics.

A video subsystem is installed to provide real time qualitative feedback of maneuvers, and as a safety measure to allow manual aircraft control where attitude determination would otherwise be difficult due to distance and aircraft size. The camera is very small (Supercircuits PC208XP, 8mm cube, 2 grams) to allow placement anywhere on the airframe with minimal impact to aerodynamics or mass properties.

B. GenMAV 1 Flight Testing

Initial flight testing of GenMAV 1 was used to assess the control power of the elevons, evaluate the center of gravity, set the autopilot gains, and practice test maneuvers. Launches were accomplished by hand launching; landings were performed by skidding into a grass covered area.

A series of doublet and pulse maneuvers, along with a 360° barrel roll and gliding flight segment, were selected to characterize the GenMAV 1 flight dynamics. Descriptions of these maneuvers are presented in Table 1. Flight test data for test points B, D, and K are presented in Figure 2. These same maneuvers will be used in subsequent flight tests.

Table 1. Series of flight test maneuvers to characterize the GenMAV vehicle.

TEST POINT	MANEUVER	DESCRIPTION
A	Pitch Doublet – ½	Positive ½ deflection for 1 sec, negative ½ deflection for 1 sec, release control stick
B	Pitch Doublet – Full	Positive full deflection for 1 sec, negative full deflection for 1 sec, release control stick
C	Roll Doublet – ½	Left ½ deflection for 1 sec, right ½ deflection for 1 sec, release control stick
D	Roll Doublet – Full	Left full deflection for 1 sec, right full deflection for 1 sec, release control stick

E	Pitch Pulse Fwd – ½	Positive ½ deflection for 1 sec, release control stick
F	Pitch Pulse Back – ½	Negative ½ deflection for 1 sec, release control stick
G	Pitch Pulse Fwd – Full	Positive full deflection for 1 sec, release control stick
H	Pitch Pulse Back – Full	Negative full deflection for 1 sec, release control stick
I	Roll Pulse Right – ½	Right ½ deflection for 1 sec, release control stick
J	Roll Pulse Right – Full	Right full deflection for 1 sec, release control stick
K	360° Roll Right – Full	Right full deflection, complete 360° roll
L	Gliding Descent	Set throttle to 0%, maintain state for 5 sec

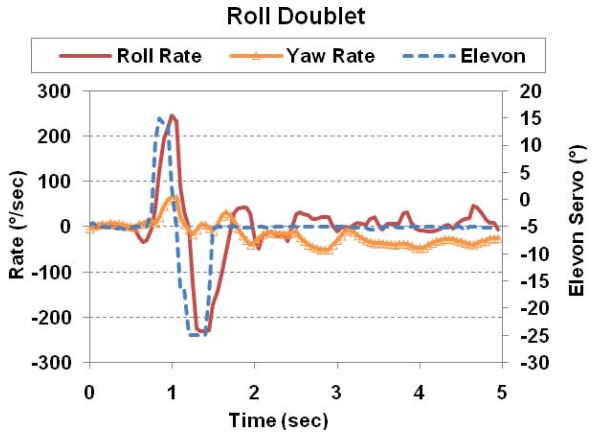

a) Control surface command and lateral body rates during a pure roll maneuver

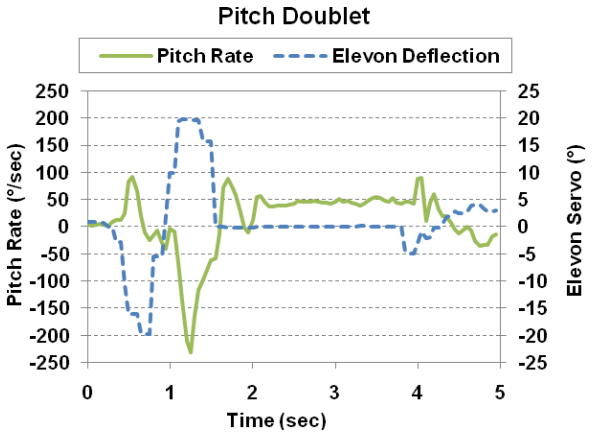

b) Control surface command and pitch rate during a pure pitch maneuver

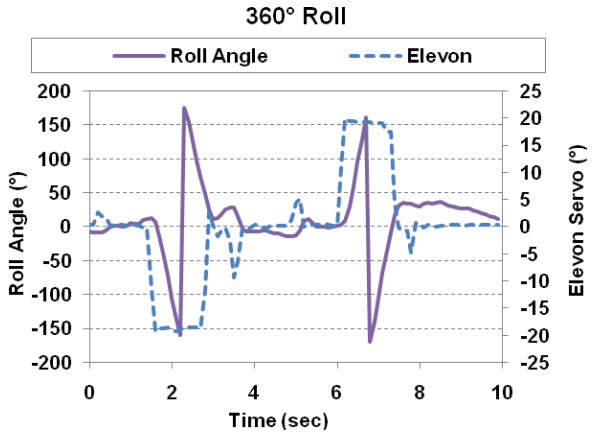

c) Control surface command and roll angle for a full roll maneuver

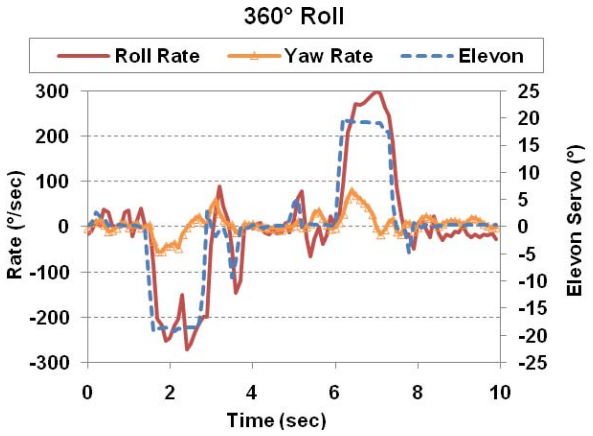

d) Lateral body rate response during a full roll maneuver

Figure 2. Flight test data for GenMAV 1.

III. Single-Jointed Articulated-Wing Configuration

A single-jointed wing is used to begin the study of an articulated-wing for purposes of gust alleviation. This configuration is the simplest, meaning it is the easiest to construct and to simulate, providing a good starting point from which to iterate. The vehicle design is like that of GenMAV 1, having the same high-wing design, wingspan, and tail size. For this reason, this vehicle will be designated as "GenMAV 2". Some modifications were made to the fuselage to accommodate the mechanism for allowing wing-articulation. The fuselage diameter is 3.4" at its widest point and the length of the fuselage is extended by 1". The fuselage is constructed of three plies of [0/90] woven carbon fiber with a fourth ply inserted to locally stiffen the wing roots. Additional structures including the battery tray serve to add additional stiffness at the wing root. Tail configuration and sizing were kept the same based on the stability and ease of manual control of GenMAV 1. The layup of the GenMAV 2 wing was with the same mold as that of GenMAV 1 but with four plies in a $[45, 45/0, 90]_s$ configuration. This gave the wings a higher degree of stiffness in all load conditions, but particularly in torsion. Also, a "spar" of 4-40 threaded steel was inserted at approximately the quarter chord to facilitate attachment of the spring /damper mechanism. Top and side views of the GenMAV 2 are given in Figure 3. Note the camera placed on the vertical tail surface to monitor wing movement during flight.

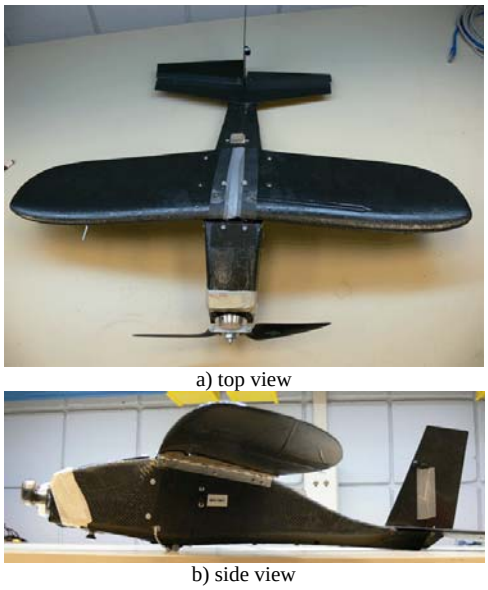

a) top view

b) side view

Figure 3. Flight-ready GenMAV 2.

A. Wing-Fuselage Joint and Spring Mechanism

Piano hinges are used to connect each wing to the fuselage and limit the wing motion to deflect in dihedral / anhedral only, as seen in Figure 4. A shock is connected to the wing root and the interior bottom of the fuselage. At the wing root, a ball joint is attached to the threaded "spar" allowing a variation of the moment arm if necessary and freedom of movement as the wing articulates. The lower ends of the spring/dampers are fixed to the bottom of the fuselage with a pin and rubber grommet which restricts movement to less than a few degrees in any direction. This allows the change in dihedral angle to be modeled as a spring-damper system. A potentiometer is connected to each wing root to measure the wing deflection. Figure 5 shows the corresponding shock and potentiometer for the left wing.

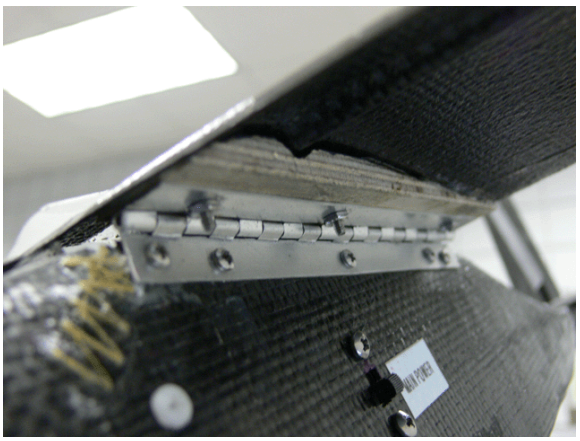

Figure 4. Piano hinge forming the joint between the left wing and fuselage of GenMAV 2.

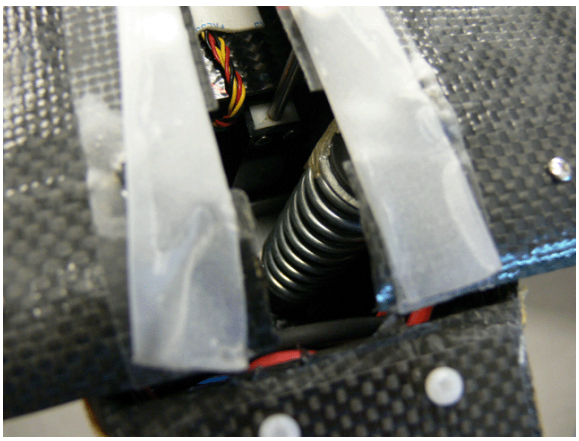

Figure 5. Top view of shock and potentiometer corresponding to the left wing of GenMAV 2.

The stiffness of the wing shocks can be varied by replacing the springs and was chosen such that the wings would have a 0° dihedral when the vertical load factor is 1. When not in flight, the wings rest at a negative dihedral, as seen in Figure 6. The dampers used are TRAXXAS 3762A radio control truck shocks with a fixed damping rate

and oil filled cylinders. The springs are steel with a spring rate of 10.64 kg/cm (59.57 lb/in), an outer diameter of 2.06 cm (0.812 in) and a wire diameter of 0.267 cm (0.105 in). The whole spring / damper was epoxied together to allow for loading in tension as well as compression.

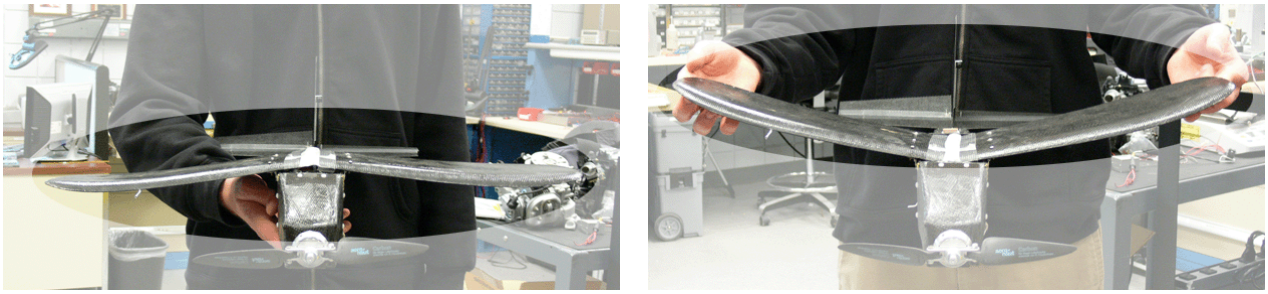

a) Negative dihedral when aircraft is at rest. b) Positive dihedral created by load acting on wings.

Figure 6. Demonstration of wings to rotate about piano hinges on GenMAV 2.

B. GenMAV 2 Flight Testing

GenMAV 2 underwent the same flight test maneuvers as GenMAV 1. Refer to Table 1 for a description of these maneuvers. Video footage from the initial flight tests of GenMAV 2 shows the wings experiencing both dihedral and anhedral during maneuvers and wind gusts. Further flight testing was conducted with a plate affixed between the wings to restrict wing articulation. This allowed comparison of fixed wing data from the same flight vehicle, as it was noticed that the thin wings of GenMAV 1, originally designed to be rolled for storage and easy transportation, are flexible in torsion and do not have the same dynamic flight characteristics as that of the GenMAV 2, even in its fixed-wing configuration. Data from the fixed-wing flight test is presented in Figure 7. Additional flight tests of the fixed-wing vehicle will be used to validate a digital simulation that models GenMAV 2. Validating this simulation is important as it will be the baseline for modeling the articulated-wing prototype and derivations thereof.

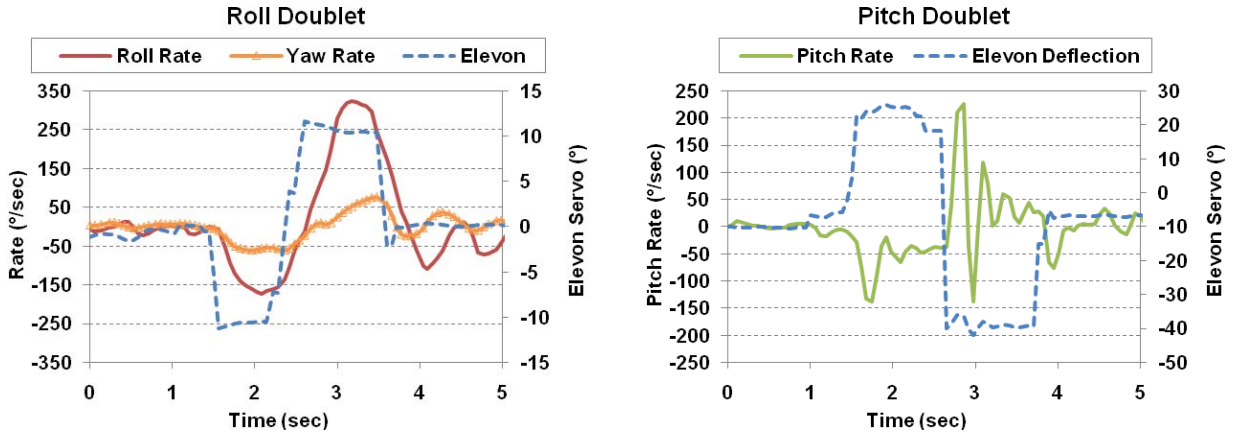

a) Control surface command and lateral body rates during a pure roll maneuver a) Control surface command and lateral body rates during a pure pitch maneuver

Figure 7. Flight test data for the fixed-wing configuration of GenMAV 2.

Initial system identification of the GenMAV 2 was completed using output error method (OEM) software in conjunction with predictions from a vortex lattice code, AVL[9]. The algorithm for the output error method was authored by Dr. Ravindra Jategaonkar[10] of the DLR German Aerospace Center and was adapted to fit the format of the flight test data, to provide a means of selecting a smaller subset of maneuvers for analysis from a larger set, and to integrate the state equations over a finer time scale. Tables Table 2 - Table 5 show the AVL-predicted coefficients versus the coefficient values obtained from the output error method and the fixed-wing flight test data. Since the values from the OEM are based on one flight test, it would be best to collect more test data to increase the confidence in these estimates.

Table 2. Static coefficients of the fixed-wing GenMAV 2.

	C_{x0}	C_{y0}	C_{z0}	C_{l0}	C_{m0}	C_{n0}
AVL	-0.10711	0.0	-0.55426	0.0	0.25646	0.0
OEM	-0.14317	--	-0.58023	--	-0.05286	--

Table 3. Control derivatives for the left elevon of the fixed-wing GenMAV 2. Derivatives for the right elevon will be of the same magnitude and of the sign represented in ( ). Units are in rad^{-1}.

	$C_{x\delta le}$ (δre)	$C_{y\delta le}$ (δre)	$C_{z\delta le}$ (δre)	$C_{l\delta le}$ (δre)	$C_{m\delta le}$ (δre)	$C_{n\delta le}$ (δre)
AVL	-0.00917 (-)	-0.02349 (+)	-0.51967 (-)	0.03781 (-)	-0.11814 (-)	0.01066 (-)
OEM	-0.14414 (-)	-0.04489 (+)	-0.00150 (-)	0.03319 (-)	-0.11995 (-)	0.01108 (-)

Table 4. Static stability derivatives of the fixed-wing GenMAV 2. Units are in rad^{-1}.

	$C_{x\alpha}$	$C_{y\beta}$	$C_{z\alpha}$	$C_{l\beta}$	$C_{m\alpha}$	$C_{n\beta}$
AVL	0.21199	-0.43497	-4.6180	-0.15786	-0.71204	0.05035
OEM	-0.81369	-0.61816	-5.8982	-0.13106	-0.97881	0.10601

Table 5. Dynamic stability derivatives of the fixed-wing GenMAV 2. Units are in rad^{-1}.

	C_{xq}	C_{yp}	C_{yr}	C_{zq}	C_{lp}	C_{lr}	C_{mq}	C_{np}	C_{nr}
AVL	-0.81696	-0.1130	0.23718	-8.1553	-0.45343	0.16826	-15.007	-0.02499	-0.14474
OEM	--	-1.2347	0.66355	--	-0.44807	0.37106	-12.776	0.17245	-0.49483

IV. Data Analysis

Data sets from the fixed and articulated-wing test flights of GenMAV 2 were plotted and a comparison made between the dynamic responses of the two wing configurations. It was noted that the pitch rate and normal acceleration response was reduced for the articulated-wing configuration during the pitch doublets. The effect is more apparent for the full-deflection doublet than for the half-deflection. This is seen in Figure 8 where the difference between the 30° doublets is more pronounced than the 15° doublets. To better visualize this trend, the magnitude of the response versus the elevon deflection is plotted in Figure 9. For the larger deflections, the articulated-wing response is approximately half that of the fixed-wing response. The reduction in normal acceleration appears to correspond with the change in wing dihedral. This is portrayed in Figure 10, where the movement of the wing results in a lower magnitude of normal acceleration than seen in the fixed-wing configuration.

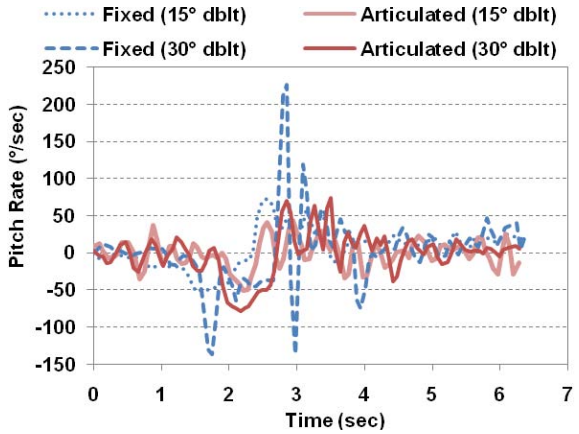

a) Pitch rate response to doublets at 15° and 30° elevon deflection

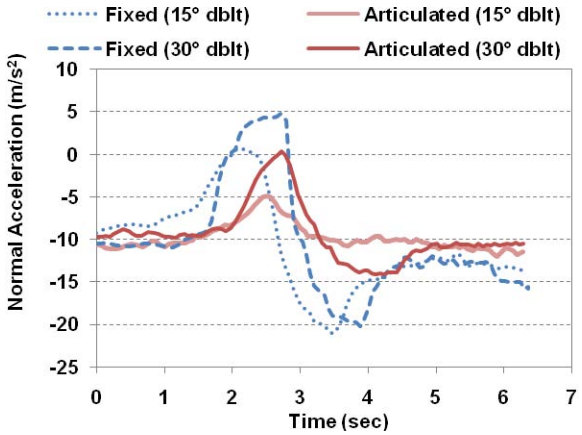

b) Normal acceleration response to doublets at 15° and 30° elevon deflection

Figure 8. Time-history comparison of the response between the fixed and articulated-wing GenMAV2 during two different pitch doublets.

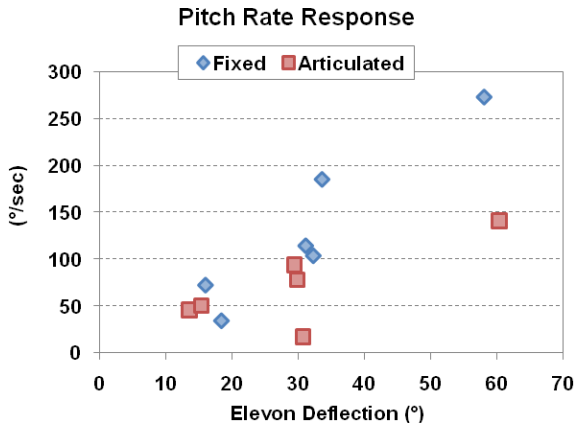

a) Magnitude of the pitch rate response to doublets at 15° and 30° elevon deflection

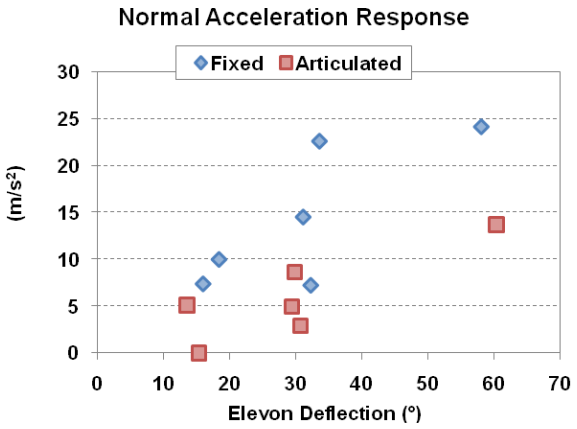

b) Magnitude of the normal acceleration response to doublets at 15° and 30° elevon deflection

Figure 9. Comparison of the response magnitude between the fixed and articulated-wing GenMAV 2 during two different pitch doublets.

While the response to a pitch disturbance is smaller in magnitude for the articulated-wing configuration, the opposite is observed during a roll doublet. A comparison between the two wing configurations shows an increase in the roll response. There is no observed difference in the yaw rate or lateral acceleration response. This comparison is shown in Figure 11. A plot showing the magnitude of the response versus elevon deflection is provided in Figure 12, where roll doublets from two separate flight tests of the articulated wing are displayed. As observed during the pitch doublets, the difference in response magnitude corresponds with the change in dihedral, as seen in Figure 13.

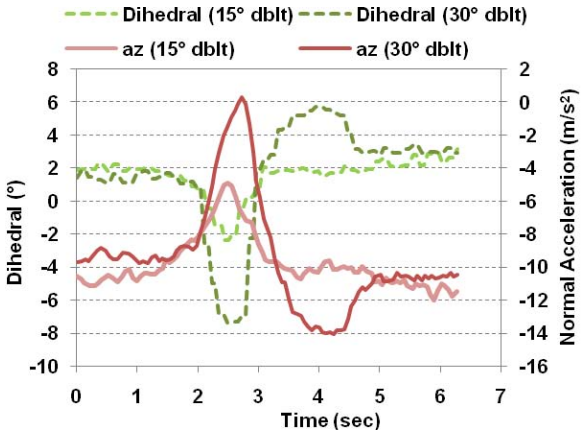

Figure 10. Time history of the correlation between the normal acceleration and the wing dihedral during two pitch doublets.

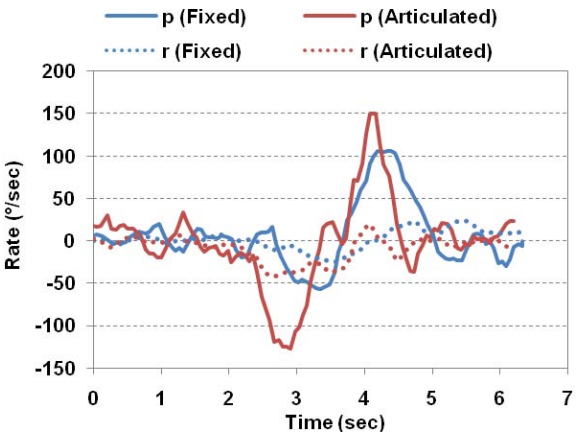

a) Roll and yaw rate response to doublets at 15° and 30° elevon deflection

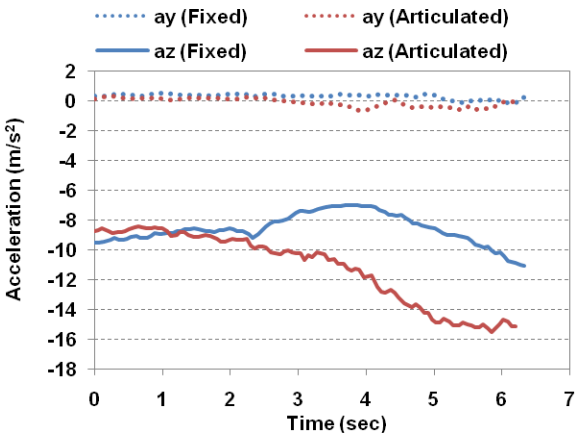

b) Lateral and normal acceleration response to doublets at 15° and 30° elevon deflection

Figure 11. Time-history comparison of the response between the fixed and articulated-wing GenMAV 2 during a roll doublet.

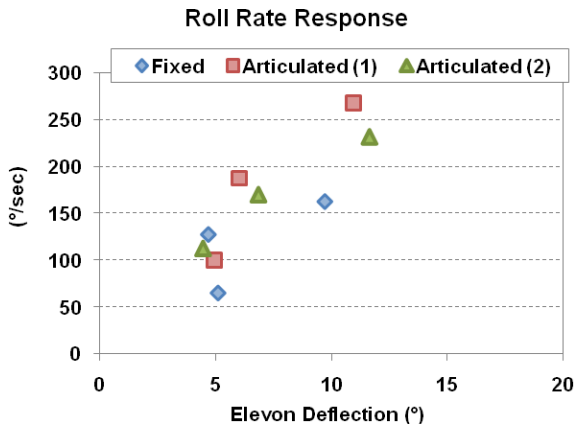

Figure 12. Comparison of the response magnitude between the fixed and articulated-wing GenMAV 2 during a roll doublet.

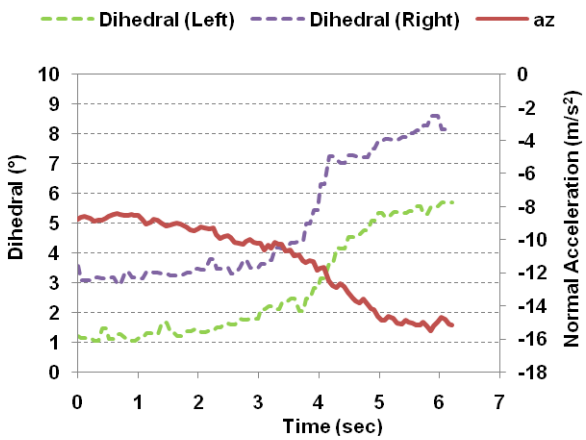

Figure 13. Time history of the correlation between the normal acceleration and the wing dihedral during a roll doublet.

The results presented suggest that further flight testing of the GenMAV 2 should be pursued. Specifically, the same test maneuvers should be executed, but the control inputs should be programmed for consistency. An example of the inconsistency in elevon deflection for the pitch doublets is displayed in Figure 14. Programmed control inputs will lend repeatability to the test maneuvers and provide cleaner comparison between tests of the two wing configurations. The fixed-wing flight test data will also be used to validate an existing simulation of the fixed-wing configuration, from which the articulated-wing simulation will be developed. The use of programmed control inputs to obtain flight data for purposes of system identification has been shown to be successful in the testing of other unmanned aerial vehicles.

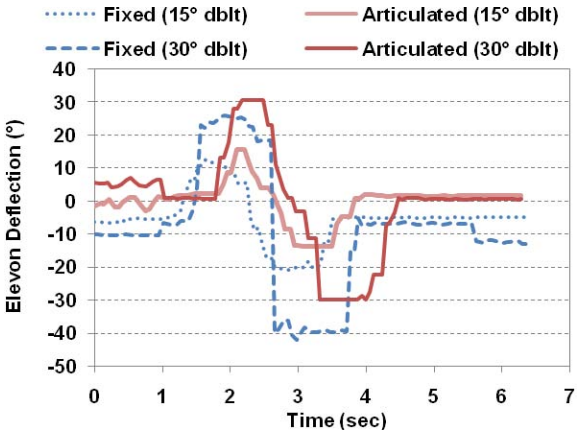

Figure 14. Time history of the elevon deflection during pitch doublets of the fixed and articulated-wing flight tests.

V. Conclusion

This paper presents a single-joint, articulated-wing MAV prototype, GenMAV 2, and the results of its initial flight tests. The focus of the paper is on the design and flight characteristics of the vehicle and how the vehicle contributes to the study of using passive wing deformation for wind gust alleviation. Of particular interest is the effect of passively-deforming wings with respect to vehicle stability and control. Data from the flight tests of GenMAV 2 show a reduction in response to pitch disturbances for the articulated-wing configuration. This reduced response to a pitch disturbance suggests the idea of using passive wing deflection to cope with wind gust disturbances. Additional flight testing of both the fixed and articulated-wing vehicles will be pursued to better observe the effects of the articulated-wing and obtain data suitable for system identification. The GenMAV 2 prototype will be the first iteration towards a final design of an articulated-wing MAV that provides further insight into the flight and control of flexible-wing MAVs.

Acknowledgements

The authors would like to acknowledge the technical contributions of Mr. John Krieger and Mr. Johnny Walker, Air Force Research Laboratory, Munitions Directorate, for their help in building and flight testing of the MAV models described herein.

References

[1] Ol, M., Parker, G., Abate, G., and Evers J., "Flight Controls and Performance Challenges for MAVs in Complex Environments," AIAA Paper 2008-6508 presented at the Guidance, Navigation, and Controls Conference, Honolulu, HI, August 2008.

[2] Albertani, R., Stanford, B., Hubner, J. P., and Ifju, P.G., "Aerodynamic Coefficients and Deformation Measurements on Flexible Micro Air Vehicle Wings", Mechanical and Aerospace Engineering Department, University of Florida, Gainesville, FL, 2007.

[3] Ifju, P., University of Florida, personal communication.

[4] Song, A. and Breuer, K., "Dynamics of a compliant membrane as related to mammalian flight," AIAA paper, 2007-0665. AIAA Aerospace Sciences Meeting, Reno NV 2007.

[5] Rojratsirikul P., Wang, Z., and Gursul, I., "Unsteady Aerodynamics of Membrane Airfoils," AIAA paper 2008-0613, AIAA Aerospace Sciences Meeting, Reno NV 2008.

[6] Stewart, K., Wagener, J., Abate, G., and Salichon, M., "Design of the Air Force Research Laboratory Micro Aerial Vehicle Research Configuration," *AIAA 45th Aerospace Sciences and Meeting Exhibit*, January 2007.

[7] Stewart, K., Abate, G., and Evers, J., "Flight Mechanics and Control Issues for Micro Air Vehicles," *Atmospheric Flight Mechanics Conference*, AIAA, August 2006.

[8] DeLuca, A., Reeder, M., Ol, M., Freeman, J., Bautista, I., and Simonich M., "Experimental Investigation into the Aerodynamic Properties of a Flexible and Rigid Wing Micro Air Vehicle," AIAA Paper 2004-2396, June 2004.

[9] AVL, Athena Vortex Lattice, Software Package, Ver 3.26, Drela, M. and Youngren, H., URL: http://web.mit.edu/drela/Public/web/avl/ [cited 8 August 2008]

[10] Jategaonkar, R., *Flight Vehicle System Identification: A Time Domain Methodology*, Progress in Astronautics and Aeronautics Series, AIAA, Reston, Virginia, 2006, Chap. 4.

Appendix 4

Experimental Data for Micro Air Vehicles with Pliant Wings in Unsteady Conditions

This page intentionally left blank

Experimental Data for Micro Air Vehicles with Pliant Wings in Unsteady Conditions

Judson Babcock[1]
Air Force Research Laboratory, Munitions Directorate, Eglin AFB, FL

Roland Scheffer[2]
Air Force Research Laboratory, Munitions Directorate, Eglin AFB, FL

Roberto Albertani[3]
University of Florida – REEF
Mechanical and Aerospace Engineering Department, Shalimar, FL

Gregg Abate[4]
Air Force Research Laboratory, Munitions Directorate, Eglin AFB, FL

This paper describes a new system for dynamic wind-tunnel testing in relation to the estimation of the dynamic stability derivatives of micro air vehicles. The research is presented for two geometrically identical Zimmerman wing configurations: rigid and flexible. A two degrees-of-freedom rig permits the measurement of the two individual components of the rotary damping moment by manipulating the model in a pure plunging motion or a combined pitching/plunging motion. A modern design of experiments methodology was used to elucidate the correlation between the wings structural deformations and the aerodynamic damping characteristics of the rigid and flexible wings. In the case of a flexible wing, the latex membrane elastic deformations are measured using visual image correlation whereby the pre-tension strain state is characterized prior to the aerodynamic tests. Comparisons of lift and drag between the rigid and flexible wings in static and dynamic conditions showed that the flexible wing with the elastic membrane skin with medium tension provided the best lift-to-drag ratio. Specific patterns in the aerodynamic coefficients were observed in the presence of dynamic changes in angle of attack or pitch angle. The increase of $\dot{\alpha}$ and $\dot{\theta}$ is shown to be a significant factor in the responses of the MAV wing, particularly on the pitching moment coefficient.

Nomenclature

AOA	=	angle of attack [°]
C_L	=	coefficient of lift
C_D	=	coefficient of drag
C_m	=	coefficient of pitching moment
MAV	=	micro air vehicle
$\overline{q}$	=	dynamic pressure [Pa]
VIC	=	visual image correlation
α	=	angle of attack [°]
$\dot{\alpha}$	=	rate of change in angle of attack [°/s]
ε	=	strain [μm/m]
θ	=	pitch angle [°]
$\dot{\theta}$	=	rate of change in pitch angle [°/s]

[1]Aeronautical Engineer, AFRL/RWGN, 101 W Eglin Blvd, Ste 214, EglinAFB, FL 32542, AIAA Member.
[2]Electronics Exchange Engineer, AFRL/RWGN, 101 W Eglin Blvd, Ste 214, EglinAFB, FL 32542, AIAA Member.
[3]Affiliate Research Assistant Professor, University of Florida, ralb@ufl.edu, AIAA Member.
[4]Aeronautical Engineer, AFRL/RWGN, 101 W Eglin Blvd, Ste 214, EglinAFB, FL 32542, Associate Fellow.

I. Introduction.

A typical micro air vehicle (MAV) cruise flight Reynolds number is in the order of 100,000. A bio-inspired pliant-membrane wing structure design has shown clear benefits in terms of flying qualities, crashworthiness, relatively easy application of morphing capabilities and ground handling (easy stowage).[1] The physics of micro air vehicles is characterized by a large number of factors and its development is relatively immature; consequently, high-fidelity simulations do not yet exist for a generic MAV.

These highly flexible structures introduce relevant non-linear fluid-structure interactions coupled with significant propeller downwash effects, exposing new problems in the prediction of flight stability and control. The theories and available models describing the fluid-structure interactions at low speed are still embryonic and require experimental validation while the effects of unsteady flight conditions on aerodynamics and propulsion are largely unknown. This paper will describe and review wind tunnel experiments performed to investigate the aerodynamic characteristics of micro air vehicles with flexible and fixed wings in unsteady conditions. Experimental conditions include various pitching/plunging cases with combinations that will provide for the conditions of model angle-of-attack not equal to the pitch angle. A modern design of experiments approach is used to model the response of the aerodynamic coefficients to these conditions for varying levels of wind tension. Realistic experimental values of the dynamic pitch damping derivatives are obtained, along with dynamic lift and drag coefficients. Visual image correlation (VIC) is used to document the elastic pre-tension on the latex membrane of the skin of the flexible wings used in the motions.

The main target of the study is the characterization of the dynamic derivatives, especially the pitch damping derivatives. Previous research for large aircraft has identified a dependence on the dynamic parameters of rate of change in angle of attack or pitch angle at subsonic and supersonic speeds due to unsteady loading of the wing.[2] However, there has been little study of these unsteady effects on MAV wings at low Reynolds numbers, especially flexible MAV wings.[3,4] Traditionally, there is great difficulty in experimentally quantifying these effects; previous flight control studies have chosen values for the dynamic derivatives based on typical estimates instead of experimental data.[5,6] The effects of wing elasticity are also studied in static and dynamic conditions.

II. Experimental Set Up

The MAV wing used in the wind tunnel testing, illustrated in Fig. 1, is taken from the well-documented University of Florida MAV.[7] It is a typical MAV wing with a Zimmerman-type planform consisting of two ellipses meeting at the quarter chord. The rigid wing is made entirely of carbon-fiber while the flexible wing is constructed of a carbon-fiber perimeter with a latex membrane stretched over the interior. The rigid and flexible wings share the same shape, size, and curvature, with a chord length of 125 mm, wingspan of 150 mm, camber at the root of 3.50 mm, and an area of 0.0178 m^2. All pitching moment data is referenced to the quarter-chord point.

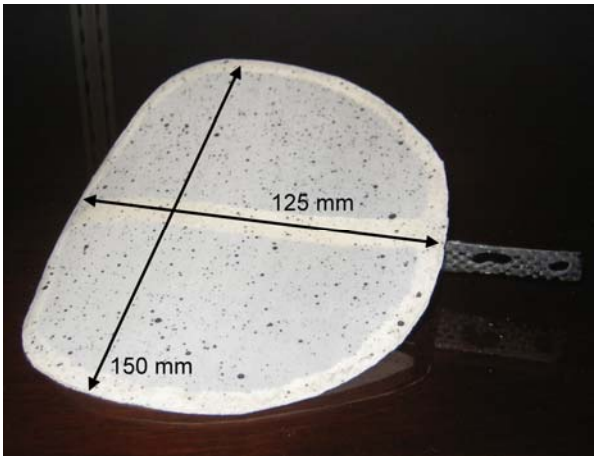

Figure 1. A 150 mm wingspan pliant MAV wing. *The pliant wing is made of latex skin with carbon fiber perimeter reinforcement.*

Figure 2. The MAV wing in the wind tunnel. *The model is attached to the two D.O.F. rig through the sting balance.*

The low-speed wind tunnel at the University of Florida's Research, Engineering, and Education Facility (REEF) was used to conduct these experiments.[8] The open-loop, open-jet wind tunnel is capable of speeds ranging from 0 – 22 m/s with turbulence levels below 0.16%. The test section has an axial length of 10 feet with 42" square opening surrounded by a structural enclosure. The specifics of the wind tunnel capabilities, flow uniformity, and turbulence have been extensively documented in reference 8. A typical installation of the MAV wing in the wind tunnel is illustrated in Fig. 2.

A two-degrees-of freedom motion rig, shown in Fig. 3, was designed for the requirements of wind tunnel testing conditions with the model angle of attack (AOA) not equal to the pitch angle (simulating dynamic motions such as rotation, plunging, and pitching). The main components are two ironless magnetic linear motors connected to two drivers and a Galil motion controller[9] operating together as a closed loop system. The linear motors have a carriage travel distance of 0.76 m. Each one is capable of speeds up to 5 m/s and can move to a commanded position with a resolution of 5 μm. The maximum acceleration of each linear motor is 6 g with a continuous force of 663.7 N and a peak force of 2967.2 N. The rig, as illustrated in Fig. 3, has two 1.5 m aluminum vertical arms holding a 0.38 m high modulus steel rod with a sleeve connection to allow for rod rotation. The sting balance is mounted on the steel rod. The mutual position of the two linear motors determines the rod angle thus the model attitude; the nominal angle test range of ±30 degrees can be extended by mechanical add-on devices.

Force and moment data are measured through a six-component strain-gauge sting balance. Two different size balances are available in the facility. The larger balance is capable of measuring a maximum balance load of 4.450E+01 N normal force and 2.225E+01 N axial force with a resolution of 1.112E-01 N and 8.900E-03 N respectively and is used in the current experiment. The smaller balance can measure up to 1.335E+01 N normal force and 8.900E+00 N axial force with a resolution of 3.560E-02 N and 4.450E-03 N respectively. Both balances were calibrated to obtain 6x39 calibration matrices that resolve second and third order force interactions. The wind tunnel flow velocity is monitored by a pitot probe installed in the inlet of the test section, and the air temperature is monitored by a resistance temperature detector (RTD) sensor mounted on the inside of the test section. Readings from those sensors are stored in the results file.

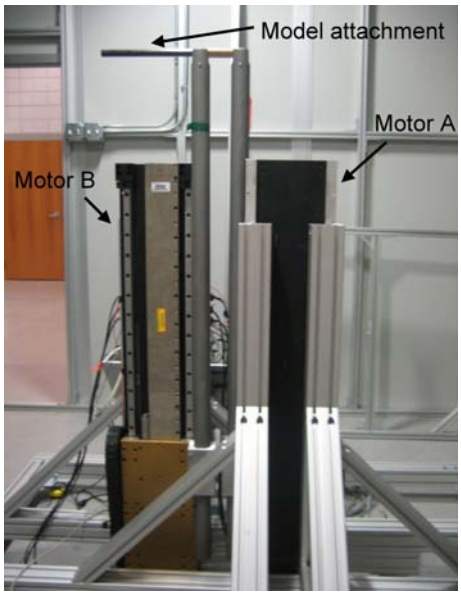

Figure 3. Two degrees-of-freedom test rig

A dynamic stereoscopic VIC system using synchronized twin cameras is used to measure the tension in the flexible wings. The system uses stereo triangulation to recover 3D data from the calibrated two-camera system, with a range of measurement from 0.05% - 500% strain on a specimen size as small as 1mm.[10] Reference images were taken of the unstretched latex membrane, followed by images taken after the latex membrane was applied to the wing. The sequential images are compared using cross-correlation techniques to obtain the displacement field and strain of the latex membrane in both the x and y direction at all points on the interior of the wing. These data were averaged to obtain the mean strain in the x and y directions for variation of wing tension.

III. Methodology

The newly implemented two degrees-of-freedom dynamic rig allows for various dynamic cases of pitching and plunging with distinct values of $\dot{\alpha}$ and $\dot{\theta}$. In the $\dot{\alpha}$ case, illustrated in Fig. 4, the pitch angle of the model is held constant and the model is subjected to a plunging motion with a linear acceleration, thus producing a linear variation in the angle of attack. Different slopes are achieved by sweeping combinations of the vertical velocity profile (linear acceleration) and the wind tunnel free stream velocity. Figure 4 shows the time history of the position of the motors and the relevant angles. The second case is the $\dot{\theta}$ case, also illustrated in Fig. 4, in which the pitch angle is varied during the plunge in relationship to the plunge acceleration, resulting in a constant angle of attack during the plunge. A proof of this experimental technique was the focus of a previous project[11] and the current work will extend the experimental technique to determine the relationship between the relevant aerodynamic parameters and the rate of change of angle of attack and pitch angle.

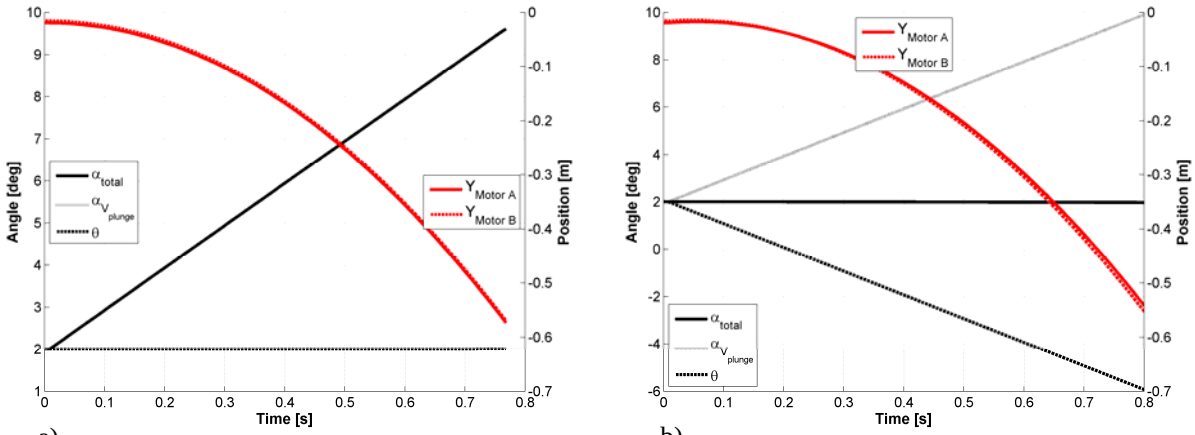

Figure 4. Combined plot with model angle of attack, pitch angle, and motor position versus time. *Left)* $\dot{\alpha} = 10°/s$ *case (pure plunge). Right)* $\dot{\theta} = 10°/s$ *case (pitching/plunging). The position of the model is displayed in red on the right axis.*

A modern design of experiments approach was used in determining the effect of the input factors, especially $\dot{\alpha}$ and $\dot{\theta}$, on the response variables (C_L, C_D, and C_m) via a polynomial relationship. Additionally, the interaction effects between factors may be discovered and analyzed. A face-centered central composite design was devised with eight center points to test for non-linearity.[12] The first experiment was designed to analyze the rigid MAV wing and included four factors (α, $\dot{\alpha}$, $\dot{\theta}$, and $\bar{q}$); the range of values listed in Table 1. Note that it was not the objective of this research to determine and compare stall angles and corresponding C_{Lmax} values; the experiment remained in the linear portion of the lift curve. The range of dynamic pressure corresponds to a free stream velocity from 8 to 13 m/s and Reynolds numbers from 68,000 to 110,000. This resulted in an orthogonal design consisting of 30 runs with no aliasing between factors.

Table 1: Experiment factors with their respective ranges

Factor	Low Value	High Value
α [deg]	0	15
$\dot{\alpha}$ [deg/s]	0	20
$\dot{\theta}$ [deg/s]	-20	0
$\bar{q}$ [Pa]	39.2	103.5
ε [μm/m]	13000	60000

In the second part of the research, the wing tension of the perimeter-reinforced wing was introduced as a fifth factor. The average strain across the latex membrane was used as the wing tension factor, at levels of 13,000, 33,000, and 60,000 microstrain (μm/m). This experimental design consisted of 50 runs.

The general equation for the response as a function of the factors is shown in Eq. (1). Effects higher than second order were not observed or modeled.

$$f(\alpha,\dot{\alpha},\dot{\theta},\bar{q},\varepsilon) = a_0 + a_1\alpha + a_2\dot{\alpha} + a_3\dot{\theta} + a_4\bar{q} + a_5\varepsilon + a_6\alpha\dot{\alpha} + a_7\alpha\dot{\theta} + a_8\alpha\bar{q} + a_9\alpha\varepsilon + a_{10}\dot{\alpha}\dot{\theta} + a_{11}\dot{\alpha}\bar{q} + a_{12}\dot{\alpha}\varepsilon + a_{13}\dot{\theta}\bar{q} + a_{14}\dot{\theta}\varepsilon + a_{15}\bar{q}\varepsilon + a_{16}\alpha^2 + a_{17}\dot{\alpha}^2 + a_{18}\dot{\theta}^2 + a_{19}\bar{q}^2 + a_{20}\varepsilon^2 \quad \textbf{(1)}$$

A reverse kinematic model was used to obtain the desired $\dot{\alpha}$ or $\dot{\theta}$ for each run. Since the result is dependent upon dynamic pressure, an iterative approach was used. For the $\dot{\alpha}$ motion, the model was plunged with a linear acceleration to produce a linear change in AOA. For the $\dot{\theta}$ motion, the angle of the model was varied during the plunge to counter the component of velocity induced by the plunge acceleration. This process was used to numerically determine the time history of each motor position during the motion. The motion was then converted into a linear motion controller program that can be executed by the user.

A Labview program was developed to control the execution of the individual runs. Acting as an interface between the dynamic motion rig, the sting-balance, and the wind tunnel, Labview was used to automatically control the execution of the motion while a hardware trigger was used to signal the balance data acquisition at the same point in each motion. In this manner, multiple cycles of each test were conducted with minimal human intervention, while maintaining the ability to reliably align data from multiple cycles. Data was acquired from the sting-balance at a sampling rate of 1 kHz.

For the wind-off tare, each motion was run using an equivalent mass at the same moment arm as the respective MAV wing. In both the wind-on and wind-off cases, each motion is repeated numerous times to enable ensemble averaging. The motion cycle is repeated five times in the wind-on case and three times in the wind-off tare. The number of cycle repetitions was the result of an analysis of the changing mean versus the number of test cycles and an effort to reduce the total number of required cycles for the experiment. With these repetitions, the combined test matrix for all wings consisted of 80 distinct motions and 640 runs. After ensemble averaging is applied, the data are filtered using a 4th order Butterworth filter with a normalized cutoff frequency of 10 Hz.

The elastic deformation of the wings, thus their shape and aerodynamics, are affected by the pliant membrane mechanical characteristics and pre-strain state. When a load is applied to the membrane, caused by the pre-tension during assembling, it introduces a de-facto new variable that needs to be accounted by measuring the plane-strain conditions of the pliant membrane. The plane-strain field is defined by the three strains ε_{xx}, ε_{yy}, and ε_{xy} acting parallel to the wing's surface. The wing's thin membrane is characterized by a plane-stress state in which the two-dimensional stress tensor generates a three-dimensional strain tensor. Effort was made to quantify the strain state in wind-off conditions with three levels of strain. The respective plain-strain distributions are illustrated in Fig. 5 showing the average values of ε_{xx} in the order of 60,219 and 12,985 μm/m in the case of high and low pre-tension membrane wings, respectively. The wind-off strain distribution, considered as a structural boundary condition, is used to characterize the wing stiffness and for correlations with its aerodynamic characteristics.

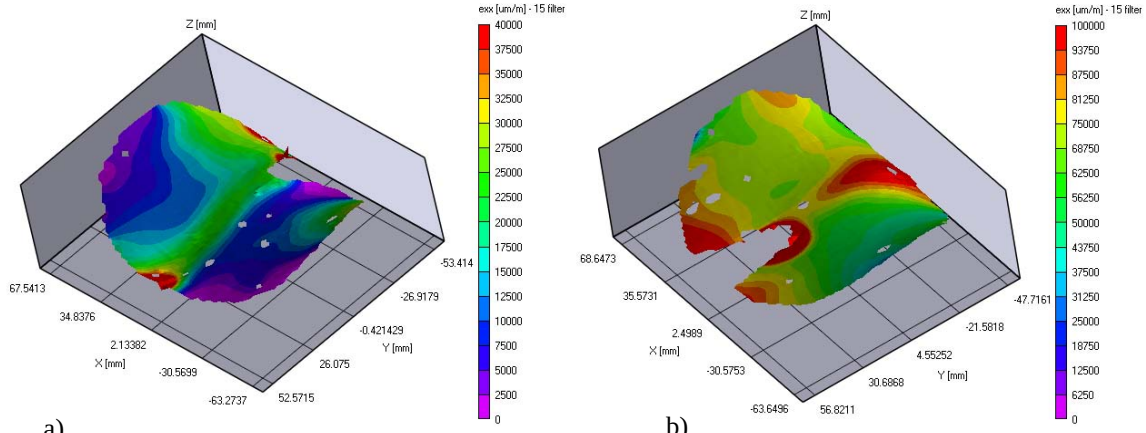

Fig. 5. Contour plots showing the wings elastic membrane strain state in the X direction for wind-off conditions. *The strains are: low-tension case (left) and high-tension case (right). The values are in microstrain (μm/m).*

IV. Results

After following the procedures outlined above, the trends of the data obtained for the individual runs are characterized by low noise levels and smooth time histories. A sample of the results for the lift coefficient of the flexible wing is shown in Fig. 6. From the left, the time history of the lift coefficient for the low-tension flexible wing during an $\dot{\alpha}$ case is shown, with the angle of attack varying linearly from -4° to 5° at a free stream velocity of 13 m/s (Re = 110,000). This represents an $\dot{\alpha}$ of 20 °/s over the duration of the plunge (0.45 seconds). The linear response of the lift coefficient is clearly seen, reaching a maximum value of 0.77 around 5° AOA. Also illustrated in Fig. 6 is the time history of the lift coefficient during the $\dot{\theta}$ case, where the angle of attack is held approximately constant at 15° during a plunge with a linear acceleration. This motion represents the $\dot{\theta}$ = -20 °/s case. This results in a relatively steady lift coefficient of 1.2 during the relevant portion of the motion.

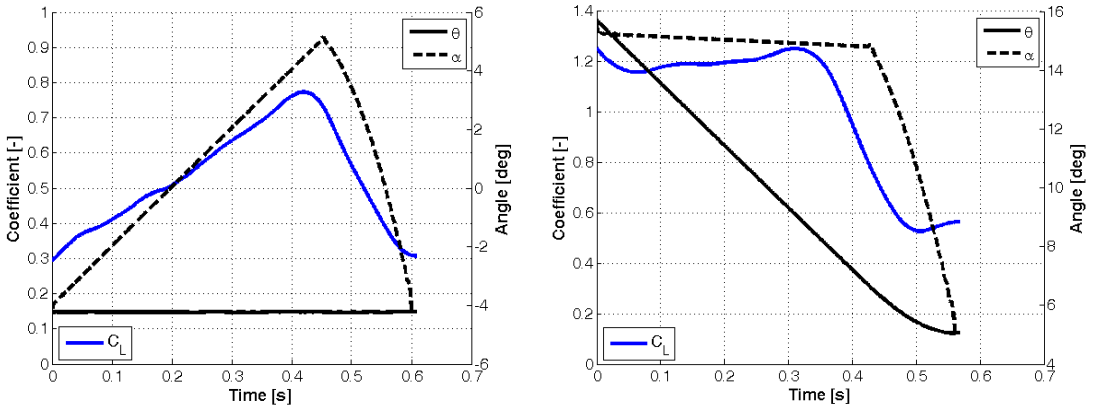

Fig. a) t coefficient time histories. *The plots represent the* b) $20°/s$ *case (a) and the* $\dot{\theta} = 20°/s$ *case (b) for the low-tension flexible wing.*

A linear model was used to analyze lift and pitching moment coefficients, whereas a square root transformation was used to analyze drag coefficient. For both wings, the regression models for lift, drag, and pitching moment fit the data very well. Residuals were random and stayed within acceptable limits.

Values for the mathematical coefficients are given in Table 2 for both the rigid and flexible wings. The influence of $\dot{\alpha}$ and $\dot{\theta}$ are seen in the *a2* and *a3* coefficients, respectively. Additionally, the most prominent interaction effect is the interaction between $\dot{\alpha}$ and $\dot{\theta}$, represented by the *a10* coefficient. After obtaining the coefficients for the rigid and flexible wings, the model was evaluated at static conditions ($\dot{\alpha} = 0°/s$, $\dot{\theta} = 0°/s$) for reference purposes and compared to the results from static wind tunnel testing. As shown in Fig. 7, the model created from the dynamic tests compares closely to the static data for both rigid and flexible wings. Especially notable is the agreement between model and static pitching moment coefficients.

The model also elucidates the influence of the membrane tension on the aerodynamic characteristics of the flexible wing. As illustrated in Fig. 8, the maximum lift for a given angle of attack can be obtained with the medium level of flexibility (a tension of approximately 33,000 μm/m). At the highest angle of attack tested (15 °), there is a 47% increase in lift coefficient from the lowest tension (13,000 μm/m) to the medium tension. However, the response of the coefficient of drag to the wing tension changes very little at any angle of attack. The result is that there is a dramatic rise in the lift-to-drag ratio for the medium tension wing at low angles of attack.

Table 2: Values of constant model parameters

	Rigid Wing			Flex Wing		
	C_L	C_D	C_m	C_L	C_D	C_m
a0	1.86E-01	7.18E-01	-3.84E-02	5.85E-02	7.12E-01	2.98E-02
a1	4.97E-02	-1.20E-04	-1.89E-03	4.92E-02	1.19E-04	-6.53E-03
a2	7.82E-03	4.07E-04	-2.58E-04	5.38E-03	8.15E-04	-3.56E-03
a3	-1.05E-02	-1.43E-04	1.58E-03	-9.26E-03	3.31E-04	5.16E-03
a4	-2.38E-04	7.35E-05	4.11E-04	3.61E-05	2.30E-04	-9.67E-05

a5	-	-	-	2.46E-05	3.68E-07	-5.11E-06
a6	-	4.76E-05	-	-	2.87E-05	-
a7	-	-5.23E-05	-	-	-7.57E-05	-
a8	-	2.96E-05	-	-	1.99E-05	-
a9	-	-	-	-	-2.21E-08	-
a10	3.06E-04	-	-1.17E-04	-	-	-2.16E-04
a11	-	-5.92E-06	-	-	-	-
a12	-	-	-	-	9.99E-09	-
a13	-	-	-	-	-	-
a14	-	-	-	-	-	-
a15	-	-	-	-	-4.17E-09	-
a16	-	3.77E-04	-	-	5.44E-04	-
a17	-	-	-	-	-5.95E-05	-
a18	-	-	-	-	-	-
a19	-	-	-	-	-	-
a20	-	-	-	-3.68E-10	-	7.08E-11

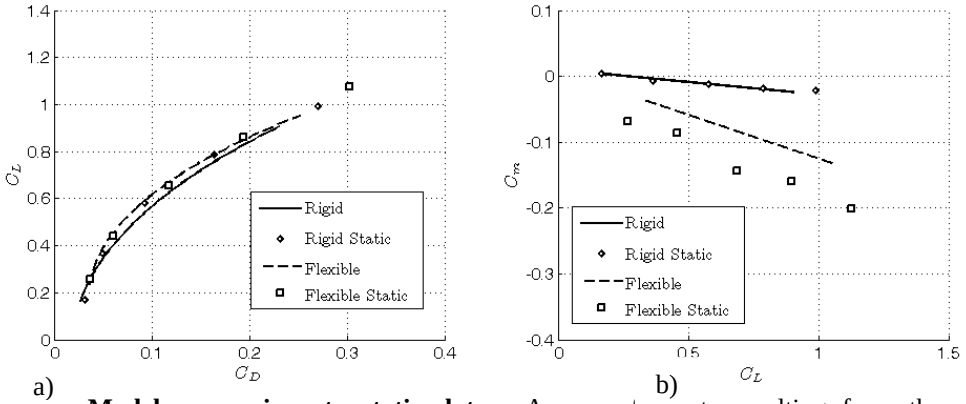

a) b)

Figure 7. Model comparison to static data. Aero coefficients resulting from the model (continuous lines) are evaluated at $\dot{\alpha} = 0°/s$, $\dot{\theta} = 0°/s$, $\bar{q}$ =103.5 Pa and compared against static wind tunnel data (discrete points). High-tension flexible wing shown.

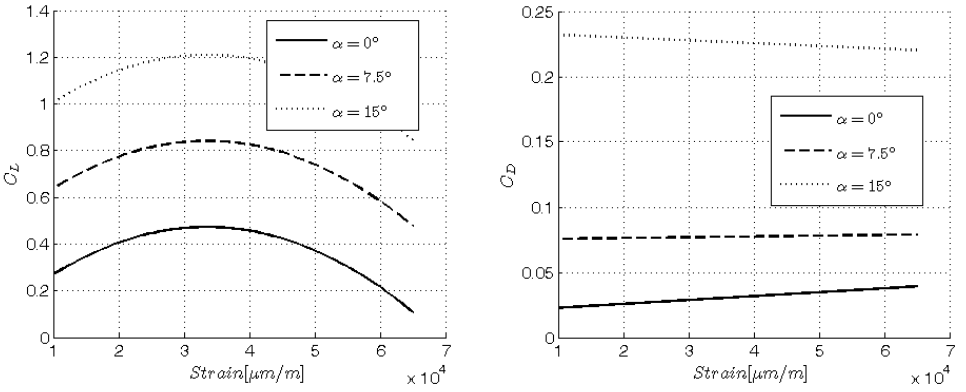

Fig. 8. Lift and drag coefficients as a function of membrane tension. Evaluated at various angles of attack, $\dot{\alpha} = 0°/s$, $\dot{\theta} = 0°/s$, $\bar{q}$ =39.5 Pa.

It was observed that the influence of dynamic pressure on the lift coefficient of the flexible wing was negligible. However, there was an influence on the drag coefficient, as seen by the presence of the *a15* coefficient in Table 2. This causes drag to increase with higher dynamic pressures, resulting in a much higher lift-to-drag ratio at low dynamic pressures (Fig. 9).

Compared to the rigid wing (Fig. 10), the medium tension wing produces a significantly higher lift-to-drag ratio at low angles of attack (in static conditions). The increase in the lift of the flexible wing can be attributed to increased wing camber from the inflation of the membrane skin due to wing loading. At the high level of tension, however, the dynamic pressure is not high enough to adequately increase the camber to obtain the same performance

as the medium tension. Furthermore, the wing section at membrane's high pre-tension level is not conforming to the design shape. With the low tension, the membrane is too loose, resulting in a non-optimal level of camber with a loss of lift and increase of drag. In this low pre-tension condition, the membrane exhibits also low frequency-high displacement vibrations.

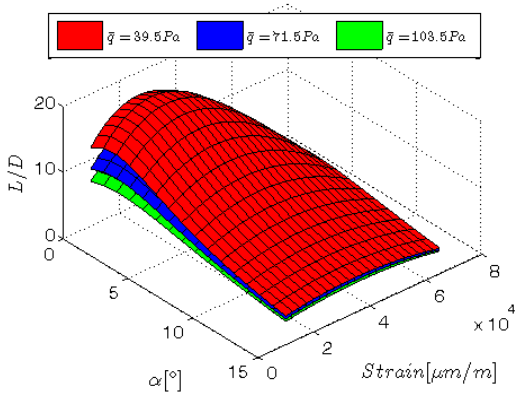

Figure 9. Response surface for the flexible wing. Shown as a function of AOA, strain, and $\bar{q}$.

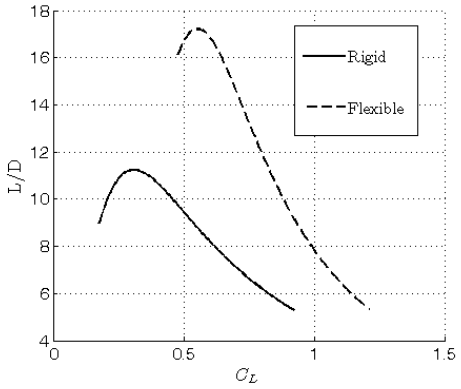

Figure 10. L/D as a function of C_L in static conditions. Medium-tension wing shown.

The behavior of the flexible wing is strongly dependent upon the dynamic conditions. As shown in Fig. 11, as the rate of change of angle of attack increases, the maximum lift coefficient also increases. For pure $\dot{\alpha}$ = 20 °/s, there is a 8% increase in lift over the static case. For pure $\dot{\theta}$ at -20 °/s, there is a 15% increase in lift over the static case. With an $\dot{\alpha}$ = 20 °/s and $\dot{\theta}$ = -20 °/s, there is a 24% increase in lift over the static case. In the drag coefficient, there is a small interaction such that the lowest drag at small angles of attack occurs at high $\dot{\theta}$ rates, but the lowest drag at high angles of attack occurs at low $\dot{\theta}$ rates.

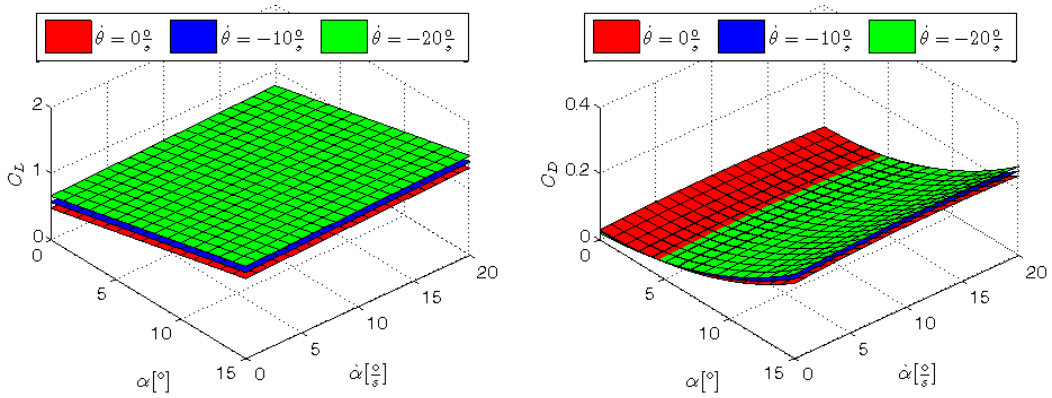

Fig. 11. Response surfaces of the medium tension flexible wing. The models are evaluated in dynamic conditions with $\bar{q}$ =39.5 Pa.

The rigid wing also experiences higher lift in dynamic conditions (Fig. 12). With a pure $\dot{\alpha}$ of 20 °/s, there is a 17% increase in lift over the static case, and for a pure $\dot{\theta}$ at -20 °/s, there is a 23% increase. With an $\dot{\alpha}$ = 20 °/s and $\dot{\theta}$ = -20 °/s, there is a 26% increase in lift over the static case. Although these percentages are greater than the flexible wing, the magnitude of the lift coefficients of the flexible wing are still higher. There is a slight interaction effect between $\dot{\alpha}$ and $\dot{\theta}$ on the lift coefficient of the rigid that can be observed via the presence of the *a10* coefficient in Table 2. There is no interaction between these factors when it comes to the drag coefficient however. The rate of change in drag coefficient due to $\dot{\alpha}$ is the same at all $\dot{\theta}$ rates, and vice-versa.

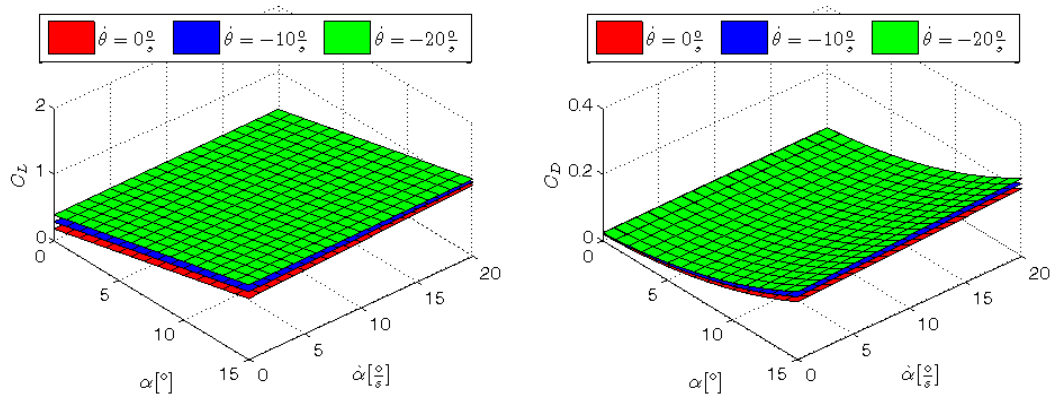

Fig. 12. Response surfaces of the rigid wing. The models are evaluated in dynamic conditions with $\bar{q}$ =39.5 Pa.

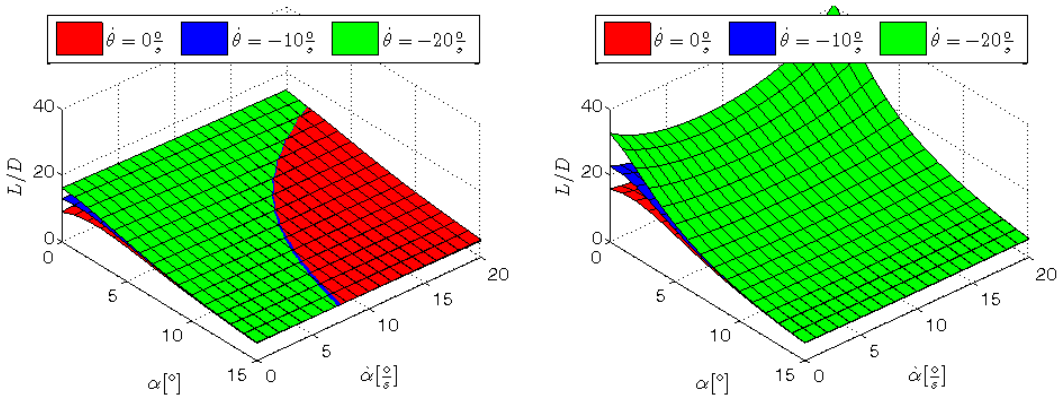

Fig. 13. Model response surfaces. The rigid wing (left) and medium tension flexible wing (right) are shown. Evaluated in dynamic conditions with $\bar{q}$ =39.5 Pa.

The increased performance in the presence of dynamic motion is best seen in the response surfaces of the lift-to-drag ratio (Fig. 13). The response of the rigid wing is heavily interacted between the dynamic parameters and produces the highest L/D ratio of 16 at $\dot{\alpha}$ =0 °/s and $\dot{\theta}$ =-20 °/s. The medium tension flexible wing produces a peak L/D of 40 at $\dot{\alpha}$ =20 °/s and $\dot{\theta}$ =-20 °/s.

The dynamic pitch damping derivatives may now be obtained by taking the partial derivative of Eq 1. and applying the model coefficients from Table 1. For both the rigid and flexible wings, the resulting pitch damping derivatives are represented in Eqs. (2-3):

$$C_{m\dot{\alpha}} = a_2 + a_{10}\dot{\theta} \tag{2}$$

$$C_{m\dot{\theta}} = a_3 + a_{10}\dot{\alpha} \tag{3}$$

From this analysis, it can be seen that the pitch damping derivates are not constant but include a strong dependence on the opposite dynamic parameter. This dependence can be observed in Fig. 14. For the rigid wing at low values of $\dot{\alpha}$, there is a 60% difference in the value for pitching moment coefficient between the minimum and maximum $\dot{\theta}$. At high values of $\dot{\alpha}$, the pitching moment coefficient varies less than 37% across the range of $\dot{\theta}$ rates. The same behavior is seen for the flexible wing, except with the additional dependence on angle of attack (Eq. 4). As seen in Fig. 14, at low $\dot{\alpha}$, there is a 283% difference between the magnitude of pitching moment coefficient at the low and high $\dot{\theta}$, but only an 8% difference at high $\dot{\alpha}$. This is a strong interaction effect in the pitching moment coefficient.

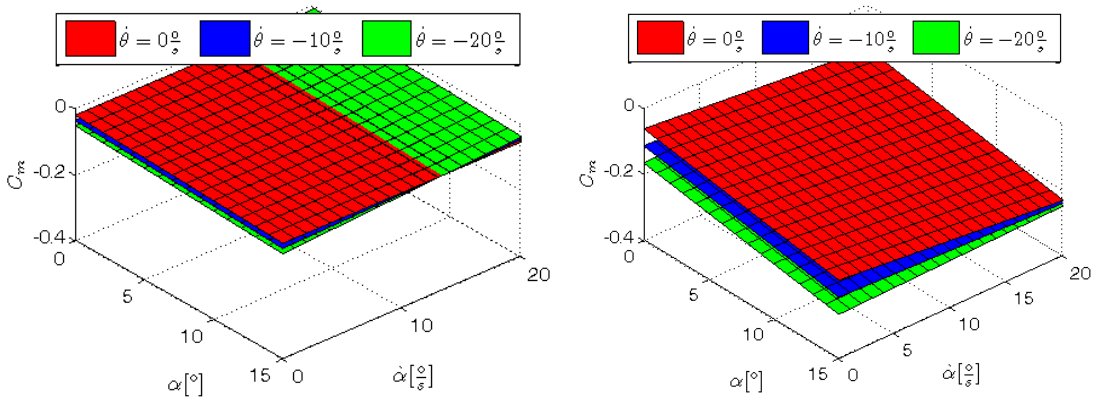

Figure 14. Model response surfaces. The pitching moment coefficient of the rigid wing (left) and the medium tension flexible wing (right) are evaluated in dynamic conditions with $\bar{q}$ =39.5 Pa.

V. Conclusions

A method has been developed and tested to determine the dependence of the aerodynamic response of a rigid or flexible MAV wing to the dynamic parameters of $\dot{\alpha}$ and $\dot{\theta}$ at low Reynolds numbers. These dynamic derivatives, especially the pitch damping derivatives, were previously unstudied for pliant MAV wings in this Reynolds regime.

The difference of lift and drag between the rigid and flexible wings in static and dynamic conditions was one of the primary observations. The medium tension flexible wing produced the highest lift-to-drag ratio when compared to the rigid wing or other levels of tension, in both static and dynamic conditions. The dependence of the lift-to-drag ratio of the pliant wing on the angle of attack was also observed.

The pitch damping derivates are not simply functions of the angle of attack, but include a strong dependence on the rate of change in angle of attack or pitch angle. Substantial changes in the aerodynamic coefficients were observed in the presence of dynamic changes in angle of attack or pitch angle. The increase of $\dot{\alpha}$, $\dot{\theta}$ has been shown to be a significant factor on the response on a MAV wing. In particular, $\dot{\alpha}$ and $\dot{\theta}$ have a dramatic influence on the pitching moment coefficient. Potential exists for improved control of a MAV, especially a flexible wing MAV, when taking into account these parameters. Further studies should be done to quantify this potential. In addition, further studies should be undertaken to expand this research to higher rates of $\dot{\alpha}$ and $\dot{\theta}$. The current experiment was limited by the restrictions of the motion rig and balance used. The resulting range of $\dot{\alpha}$ and $\dot{\theta}$ is only applicable to a small portion of the adot and tdo envelope that a MAV may see in actual flight.

Acknowledgements

asdfasdfasdfasdfasd

References.

[1] Pines, M., Bohorquez, F., "Challenges Facing Future Micro-Air-Vehicle Development," *AIAA Journal of Aircraft*, Volume 43, Number 1, March-April 2006

[2] Tobak, M., "The Use of the Indicial Function Concept in the Analysis of Unsteady Motions of Wings and Wing-Tail Combinations," NACA Report 1188, 1954.

[3] Etkin, B., Dynamics of Atmospheric Flight. John Wiley and Sons, Inc., 1972.

[4] Blakelock, J.H., Automatic Control of Aircraft and Missiles. John Wiley & Sons, Inc., 1965.

[5] Waszak, M., Davidson, J., Ifju, P., "Simulation and Flight Control of an Aeroelastic Fixed Wing Micro Aerial Vehicle," *AIAA Atmospheric Flight Mechanics Conference*, Monterey, CA, August 5-8, 2002.

[6] Waszak, M., Jenkins, L., Ifju, P., "Stability and Control Properties of an Aeroelastic Fixed Wing Micro Aerial Vehicle," *AIAA Atmospheric Flight Mechanics Conference*, Montreal, Canada, August 6-9, 2001.

[7] Albertani, R., DeLoach, R., Stanford, B., Hubner, J. P, Ifju, P., "Wind-Tunnel Testing and Modeling of a Micro Air Vehicle with Flexible Wings," *AIAA Journal of Aircraft*, Volume 45, Number 3, May-June 2008.

[8] Hart. A, et al. "Validation of a Low Reynolds Number Aerodynamic Characterization Facility," *47th AIAA Aerospace Sciences Meeting*, Orlando, FL, Jan 5-8, 2009.
[9] Galil Motion & Control. www.galilmc.com
[10] Correlated Solutions. www.correlatedsolutions.com
[11] Albertani, R., Babcock, J., "Analysis of Wind Tunnel Unsteady Aerodynamic Data of Flexible Micro Air Vehicle Wings," *26th AIAA Applied Aerodynamic Conference*, Honolulu. HI, August 18-21, 2008.
[12] Montgomery. D., "Design and Analysis of Experiments," 7th ed., John Wiley & Sons, Hoboken, NJ, 2009

This page intentionally left blank

DISTRIBUTION LIST
AFRL-RW-EG-TR-2010-001

Defense Technical Information Center — 1 Electronic Copy (1 File & 1 Format)
Attn: Acquisition (OCA)
8725 John J. Kingman Road, Ste 0944
Ft Belvoir, VA 22060-6218

EGLIN AFB OFFICES:

AFRL/RWOC (STINFO Office)	- 1 Hard (Color) Copy
AFRL/RW CA-N	- STINFO Officer Provides Notice of Publication
AFRL/RWGN	- 1 Copy
AFRL/RWAV	- 1 Copy